Article (refereed) - postprint

Lofts, Stephen; Fevrier, Laureline; Horemans, Nele; Gilbin, Rodolphe; Bruggeman, Christophe; Vandenhove, Hildegarde. 2015. **Assessment of co–contaminant effects on uranium and thorium speciation in freshwater using geochemical modelling**.

Assessment of co–contaminant effects on uranium and thorium speciation in freshwater using geochemical modelling

Stephen LOFTS[a], Laureline FEVRIER[b], Nele HOREMANS[c], Rodolphe GILBIN[b], Christophe BRUGGEMAN[c], Hildegarde VANDENHOVE[c]

[a] NERC Centre for Ecology and Hydrology, Lancaster Environment Centre, Bailrigg, Lancaster, LA1 4AP, U.K.. stlo@ceh.ac.uk

[b] IRSN, DEI/SECRE/LRE-Bât 186, B.P.3, Cadarache Center, F-13115 Saint-Paul-lez-Durance cedex, France. laureline.fevrier@irsn.fr, rodolphe.gilbin@irsn.fr

[c] Belgian Nuclear Research Centre SCK•CEN, BE-2400 Mol, Belgium. nhoreman@sckcen.be, cbruggeman@scksen.be, hvandenhove@sckcen.be

Corresponding author: S. Lofts

Abstract

Speciation modelling of uranium (as uranyl) and thorium, in four freshwaters impacted by mining activities, was used to evaluate (i) the influence of the co–contaminants present on the predicted speciation, and (ii) the influence of using nine different model/database combinations on the predictions. Generally, co–contaminants were found to have no significant effects on speciation, with the exception of Fe(III) in one system, where formation of hydrous ferric oxide and adsorption of uranyl to its surface impacted the predicted speciation. Model and database choice on the other hand clearly influenced speciation prediction. Complexes with dissolved organic matter, which could be simulated by three of the nine model/database combinations, were predicted to be important in a slightly acidic, soft water. Model prediction of uranyl and thorium speciation needs to take account of database comprehensiveness and cohesiveness, including the capability of the model and database to simulate interactions with dissolved organic matter. Measurement of speciation in natural waters is needed to provide data that may be used to assess and improve model capabilities and to better constrain the type of predictive modelling work presented here.

Keywords

Uranium; Thorium; speciation; modelling; contaminants

Abbreviations

HFO: hydrous ferric oxide

HAlO: hydrous aluminium oxide

BLM: biotic ligand model

DOC: dissolved organic carbon

DOM: dissolved organic matter

1. Introduction

Ecological risk assessment of contaminants focuses largely on exposure to contaminants singly, yet in the natural environment exposure to multiple contaminants is the norm. This is likely to be the case both for radioactive and non–radioactive contaminants. Understanding and quantifying the effects of exposure to multiple contaminants (both radionuclides and non–radioactive substances) is clearly important for improving risk assessment and is an active research area, yet prediction of the effects of multiple contaminants is as yet poorly developed. Understanding of multiple contaminant impacts needs to incorporate factors known to influence the impacts of single contaminants. An extensive body of research exists demonstrating that total or dissolved concentrations of metallic contaminants in surface waters are not generally predictive of toxic effects on biota, and that the extent of the metal toxicity is modified by other factors such as pH and the concentrations of dissolved major ions and organic matter (Franklin et al., 2000; Meyer, 2002; Markich, 2013; Trenfield et al., 2011a). This is generally accepted to be the result of chemical speciation differences in the exposure medium, coupled with competitive uptake effects, as exemplified by the Biotic Ligand Model (BLM) for metals (Paquin et al., 2002). In the conceptual framework used by the BLM, competition for the potentially toxic metal between the organism and solution ligands, such as CO_3^{2-} or dissolved organic matter (DOM), and competition among the metal and major ions for binding to the solution ligands, controls organismal uptake of the metal, and thus the toxic effects. The conceptual framework of the BLM has recently been extended to consider metal mixtures (e.g. Farley et al., 2014; Jho et al., 2011), where metal competition effects, both on solution speciation and on uptake by the organism, are taken into account.

Since many radionuclides encountered in the environment are metallic in nature, bioavailability models such as the BLM are in principle applicable to them. In developing such a model, there is a need firstly to assess the prediction of radionuclide speciation under realistic environmental conditions. Furthermore, since conditions entail exposure of organisms to multiple contaminants, there is a need to assess whether and how the presence of such co–contaminants influences radionuclide speciation. This study evaluates the influence of co-contaminants on the modelled speciation of uranium and thorium in surface waters by applying a set of speciation model frameworks to a collection of real–life examples of surface waters impacted by uranium and thorium contamination. This study places the similarities and differences among the predictions of speciation in the context of the different model frameworks and databases of thermodynamic parameters (binding constants) used. The latter is particularly

pertinent for radionuclides, given the historic effort into producing internally consistent databases of binding constants for use in thermodynamic models (e.g. Grenthe et al., 2004) and the number of different databases that consequently exist.

We have chosen uranium and thorium as the radioelements of interest given the potential for their release to the environment during mining, milling and processing operations, nuclear fuel production, power station discharges and waste storage/processing, alongside a range of potential co–contaminants (e.g.chromium, nickel, zinc) and other radionuclides (e.g. Garnier-Laplace et al., 2009; Herlory et al., 2013; Vanhoudt et al., 2012). The equilibrium speciation of uranium, including redox transformations and binding to environmentally–relevant colloidal and mineral phases (e.g. humic substances, iron(III) oxyhydroxides), has been extensively studied (e.g. Amme, 2002; Maher et al., 2013; O'Loughlin et al., 2011; Vitorge and Capdevila, 2003) and can be readily computed using geochemical speciation models (Denison and Garnier-Laplace, 2005; Vercouter et al., 2015). Equilibrium constants for uranium complexation with important freshwater ligands (e.g. CO_3^{2-}, organic matter) have been compiled into a number of databases for use with specific speciation models. Thorium speciation in freshwaters has also been studied (e.g. Moulin et al., 1992). We originally intended to include radium and polonium also. However, initial screening of the model databases showed that none contained any data on radium or polonium complex formation, thus speciation of these elements could not be simulated. We will thus focus in the results on the uranium and thorium modelling, but will also tackle the situation with respect to modelling radium and polonium speciation in the Discussion section.

It is now recognized that uranium speciation determines directly the bioavailability of uranium to living organisms. Although no clear consensus exists about the bioavailability of the different inorganic or organic uranium complexes, dissolved organic matter, water hardness and pH have been shown to modulate uranyl toxicity to various organisms due to their effect on speciation (Denison, 2004; Fortin et al., 2004, 2007; Lavoie et al., 2014; Markich, 2013; Trenfield et al., 2011a, 2011b; Zeman et al. 2008). The relationship between thorium speciation and bioavailability is less well studied though there is evidence of chemical effects on bioavailability from soil studies (e.g. Hegazy et al., 2013).

We have performed comparative uranium and thorium speciation calculations using seven different combinations of speciation model and binding constant database. Predictions of uranium speciation have been made in four real–life freshwaters impacted by discharges of uranium and other contaminants. By comparing speciation predictions in the presence and

absence of other contaminants, we assess the potential for such contaminants to impact the speciation of uranium in freshwaters. We assess the comparative predictions of the different speciation models and databases, and make recommendations for future consolidation and updating of databases.

2. Materials and methods

2.1. Geochemical speciation models

In this study we apply a number of speciation models to predict uranium and thorium speciation in freshwaters, to assess the role of co–contaminants on the speciation. In doing so, we make a number of key assumptions. Firstly, all uranium is assumed to be present as uranyl, U(VI). Secondly, we allow the modelling of uranyl and thorium binding to dissolved organic matter (DOM), if the geochemical speciation model can simulate this. Thirdly, if the model has the capacity to simulate the formation of colloidal hydrous ferric oxide (HFO) and the complexation of uranyl and thorium to its surface, this will also be taken into account. Dissolved organic matter and HFO are widely known to complex uranyl (e.g. Saito et al., 2004; Waite et al., 1994) and thorium (e.g. Nash and Choppin, 1980; Rojo et al., 2009)

Many geochemical speciation models are currently available, with differing capabilities. All models share the ability to compute the equilibrium speciation of a solution containing ions and simple ligands, without consideration of the oxidation–reduction state of the system. Additionally many models can simulate oxidation–reduction and precipitation–dissolution equilibria, and some advanced models couple equilibrium, reaction kinetics and transport modelling. Furthermore, some models can also simulate the reactions of ions with DOM and mineral surfaces such as HFO.

We have used five models in this work: the Windermere Humic Aqueous Model (WHAM7), Visual MINTEQ, CHESS, the Geochemist's Workbench, and PHREEQC.

2.2. Windermere Humic Aqueous Model (WHAM7)

The WHAM7 system is a speciation model that includes Humic Ion–Binding Model VII (Tipping et al., 2011), a discrete site/electrostatic model of cation binding to humic substances, which may be used to simulate ion interactions with DOM. Currently the model is parameterised for the binding of 46 cations (considering different oxidation states of the same element to represent different cations), including uranyl. WHAM7 also includes a surface complexation model (Lofts and Tipping, 1998) parameterised for oxides of iron(III),

aluminium, manganese and silicon, as well as a conventional submodel for speciation in the solution phase. Oxidation–reduction equilibria are not simulated. Precipitation of hydrous aluminium and iron(III) (hydr)oxides (HAlO and HFO) may be simulated. In all calculations, iron(III) was allowed to precipitate as HFO if its solubility product was exceeded. The solubility expression given by Lofts and Tipping (2011),

$a_{Fe[3+]} \cdot a_{H[+]}^{-2.49} \geq 10^{-0.52}$,

was used to check for HFO precipitation. Precipitated HFO may be allowed to have a chemically active surface that binds ions.

WHAM scenario simulations were done with two variants of the solution database:

i. The default database (simulations denoted WHAM–d). This database was originally compiled by Tipping (1994) and updated for WHAM7 to allow simulation of the formation of the uranyl complexes $UO_2(CO_3)_3^{4-}$, $UO_2(SO_4)_2^{2-}$, $UO_2(SO_4)_3^{4-}$, $UO_2HPO_4^0$, $UO_2H_2PO_4^+$, $UO_2H_3PO_4^{2+}$, UO_2Cl^+, $UO_2Cl_2^0$, UO_2F^+, $UO_2F_2^0$, $UO_2F_3^-$ and $UO_2F_4^{2-}$, and the thorium complexes $Th(CO_3)_5^{6-}$, $Th(OH)_2(CO_3)_3^{4-}$, $Th(OH)_3CO_3^-$, $ThSO_4^{2+}$, $Th(SO4)_2^0$ and $Th(SO_4)_3^{2-}$. Precipitated HFO was assumed to have a chemically active surface capable of binding protons and cations, including uranyl (UO_2^{2+} and UO_2OH^+) and thorium (Th^{4+} and $ThOH^{3+}$). Constants for the binding of uranyl and thorium to HFO were calculated using the linear free energy relationship of Lofts and Tipping (1998) (see Supplementary Information for details).

ii. A modified database allowing formation of the uranyl alkaline earth metal–carbonate complexes $MgUO_2(CO_3)_3^{2-}$, $CaUO_2(CO_3)_3^{2-}$, $Ca_2UO_2(CO_3)_3^0$, $SrUO_2(CO_3)_3^{2-}$, $BaUO_2(CO_3)_3^{2-}$, and $Ba_2UO_2(CO_3)_3^0$, and the hydroxy–carbonate complexes $(UO_2)_2(OH)_3CO_3^-$, $(UO_2)_3(OH)_3CO_3^+$ and $(UO_2)_{11}(OH)_{12}(CO_3)_6^{2-}$. (simulations denoted WHAM–m). Binding constants for the alkaline earth metal–carbonate complexes were calculated from the results of Dong and Brooks (2006), using log *K* values for the $UO_2(CO_3)_3^{4-}$ complex corrected to the experimental ionic strength using the extended Debye–Hückel equation. Updated binding constants for uranyl and thorium binding to HFO were derived by an evaluation of literature data; details of the data, fitting and parameters derived are given in the Supplementary Information.

2.3. Visual MINTEQ (VMIN) and the NICA–Donnan model

Visual MINTEQ is a development of the MINTEQA2 model (Hydrogeologic Inc. and Allison Geoscience Consultants Inc., 1999). The model combines codes for aqueous speciation,

oxidation–reduction equilibria, and mineral equilibria. It includes the NICA–Donnan model (Benedetti et al., 1995) for simulating the complexation of protons and metals to humic substances and the generalised two–layer model (GTLM) for the binding of metals to HFO (Dzombak and Morel, 1990). The NICA–Donnan implementation in Visual MINTEQ is parameterised for the binding of 23 metal species including uranyl. The GTLM binding constant database as supplied with the model does not contain constants for the binding of uranyl to HFO, therefore we added the binding constants derived by Mahoney et al. (2009) to the database.

Version 3.0 of Visual MINTEQ and the default inorganic speciation database were used for computations. The database is based on the original MINTEQA2 model database, with binding constants updated with values from the NIST thermodynamic database, version 7.0 (Smith et al., 2003), where possible. Simulations are denoted VMIN–d.

2.4. Chemical equilibrium of species and surfaces (CHESS)

CHESS (Van der Lee, 1998) combines aqueous speciation, oxidation–reduction equilibria and mineral equilibria. The model has the capability to simulate ion exchange and surface complexation on minerals and colloids. CHESS simulations were done using two solution databases: the default chess.tdb database (simulations denoted CHESS–ch) and the ctdpv3_Dong database (simulations denoted CHESS–ct). The default database is derived from the original database for the EQ3/6 speciation model. It contains parameters for ion binding to HFO using the GTLM. It also contains a small number of parameters for ion binding to humic acid; however these do not include parameters for uranyl. The ctdpv3_Dong database is based on a database released in 2004 in the framework of the *Common Thermodynamic Database Project* (van der Lee and Lomenech, 2004), which merged a review of uranyl thermodynamic data performed by Denison (2004) and the default Chess database, augmented with binding constants for the complexes $MgUO_2(CO_3)_3^{2-}$, $CaUO_2(CO_3)_3^{2-}$, $Ca_2UO_2(CO_3)_3^{0}$, $SrUO_2(CO_3)_3^{2-}$ and $Sr_2UO_2(CO_3)_3^{0}$ (Dong and Brooks, 2006; Geipel et al., 2008).

2.5. Geochemist's Workbench (GWB)

The GWB (Bethke and Yeakel, 2012) can simulate solution, oxidation-reduction and precipitation equilibria. It can also simulate ion binding to mineral surfaces, including ion exchangers (clays). Three databases for ion binding to HFO using the GTLM are available; however, none contain binding parameters for uranyl. The model does not have a submodel for ion–binding to humic substances.

GWB simulations were done using two solution databases: the Thermo.com.v8.r6+ database (simulations denoted GWB-c) and the Thermo.Minteq database (simulations denoted GWB-m). The Thermo.com.v8.r6+ database is derived from the Lawrence Livermore National Laboratory 'combined' database, version 8 release 6. The Thermo.Minteq database is the database used by version 2.40 of Visual MINTEQ.

2.6. PHREEQC

PHREEQC can simulate solution, oxidation–reduction and precipitation equilibria, ion exchange reactions and adsorption on mineral surfaces. Simulations were done using two databases: the llnl.dat database (simulations denoted PHREEQC–l) and the minteq.dat database (PHREEQC–m). Both databases contain parameters for the binding of ions to HFO using the GTLM, however neither database contains binding constants for uranyl or thorium. The model does not have a submodel for ion–binding to humic substances, although it is possible to include the Humic Ion-Binding Model in the code (Liu *et al*., 2008; Marsac *et al*., 2011). The minteq.dat database has no binding constants for thorium, therefore this combination could not be used to assess thorium speciation.

3. Model predictions of uranyl and thorium speciation

We firstly describe the freshwater scenarios used for comparative simulations. Water characteristics are presented in Tables 1 and 2.

3.1.1. Ritord

The Ritord basin is situated in the Limousin region of France and contains several closed uranium mines. Chemically treated mine waters are discharged to surface water at two locations within the catchment. For this scenario we chose a single water sample, taken on 18th June 2009, downstream of the uppermost mine water discharge (Herlory et al., 2013). The chemical treatment of the mine water comprises addition of barium chloride to precipitate radium, aluminium sulphate to co–precipitate iron and uranium, and a flocculating agent to minimise suspended solids. The system is slightly acidic, with moderate hardness, although this is elevated compared to an upstream unimpacted site, as a result of the mine water discharge. The DOC, sulphate and aluminium concentrations are also elevated. The mine discharge also increases the dissolved barium and uranium concentrations. The dissolved iron concentration is reduced downstream of the discharge, possibly due to formation and

aggregation or settling out of HFO. No measurements of thorium were available for this scenario.

3.1.2. Beaverlodge Lake

The location of the scenario is close to Uranium City in northern Saskatchewan, Canada. Past uranium mining operations have caused contamination of a number of local surface waters (lakes and streams). The scenario location is at the outflow of Greer Lake, upstream of its inflow into Beaverlodge Lake, the largest water body in the area. We used mean water chemistry data for the period July 1st 2003 to June 30th 2004, with the exception of DOC, for which a single monitored value from 2011 was used since no corresponding data were available for the earlier time period (KHS Environmental Management Group Ltd., 2004; Cameco Corp., 2011). Each determinant was the mean of between two and 11 individual samples.

The water was alkaline with moderate hardness. Mean water temperature was 1ºC. Based on the water composition (Table 2) barium is the main co–contaminant of non–radionuclide origin in the system. The dissolved organic carbon concentration was 14 mg C dm^{-3}.

3.1.3. Tajikistan

The chemical compositions of the waters were taken from data published by Skipperud et al. (2013). Two samples from around the Taboshar uranium mine were selected as scenarios. The first is a water-filled opencast mine hole (sample name Pit Lake) at the mine. The second is a sample from a stream draining from the mine tailings dump, named the 'Yellow Mountain' (sample name Yellow Mountain).

Both waters were alkaline. Hardness, calculated from measurements of dissolved magnesium and calcium, was very high (463 and 507 mg $CaCO_3$ dm^{-3} respectively). Alkalinity was not measured, but simulations using WHAM7, assuming the measured ionic charge deficit in the waters to be due to carbonates, predicted carbonate alkalinities of 207 and 257 mg $CaCO_3$ dm^{-3} respectively.

Concentrations of U in the samples were the highest in the scenarios, being 2000 µg dm^{-3} and 1100 µg dm^{-3} for Pit Lake and Yellow Mountain respectively. Concentrations of arsenic, nickel, chromium, molybdenum, selenium, manganese, thorium and zinc were also measured.

3.2. Scenario simulations

In order to provide a reasonable comparison among models, including those capable and not capable of simulating natural organic matter, we firstly computed the speciation of each

scenario without including organic matter. We then ran a second set of simulations using WHAM7 and Visual MINTEQ, including natural organic matter and allowing the formation of colloidal HFO and ion binding to its surface. In both cases, simulations were run both with and without the following co–contaminants:

Ritord: aluminium, iron(III), barium.

Beaverlodge: iron(III), nickel, copper, zinc, barium, lead.

Pit Lake and Tajikistan: manganese, iron(III), nickel, zinc, lead.

4. Results

4.1. Scope of model/database combinations for uranyl speciation

Table S1 in the Supplementary Information shows the binding constants for the inorganic uranyl solution species (complexes) in each model/database combination. The databases for CHESS–ch, GWB–c and PHREEQC–l are identical not only for the uranyl complexes which may be formed, but also have the same thermodynamic constants for their formation; thus speciation predictions using these model/database combinations should be similar if not identical. The GWB–m database is very similar to the VMIN–d database, being an older version of the same database, however VMIN–d does not have binding constants for the hydroxy–carbonate complexes $(UO_2)_2CO_3(OH)_3^-$ and $(UO_2)_3CO_3(OH)_3^+$, which GWB–m does. The binding constants for the alkaline earth metal–uranyl–carbonate complexes $CaUO_2(CO_3)_3^{2-}$ and $Ca_2UO_2(CO_3)_3^0$ also differ between the two databases.

With the exception of PHREEQC–m, all the model/database combinations simulate formation of the monomeric hydrolysis products $UO_2(OH)_n^{(2-n)}$ (n = 1,2,3 or 4), the simple carbonate complexes $UO_2(CO_3)_n^{(2-2n)}$ (n = 1,2 or 3), the sulphate complexes $UO_2(SO_4)_n^{(2-2n)}$ (n = 1 or 2), the phosphate complexes $UO_2H_nPO_4^{(n-1)}$ (n = 0, 1, 2 or 3) and the halide complexes $UO_2H_n^{(2-n)}$ (H is Cl^- or F^-, n = 1 or 2 for Cl^- and n = 1, 2, 3 or 4 for F^-). The PHREEQC–m database is generally sparser with respect to the range of complexes simulated compared to the other databases; of the monomeric hydrolysis products, it simulates only UO_2OH^+, and does not simulate formation of $UO_2SO_4^0$, $UO_2PO_4^-$ or $UO_2Cl_2^0$.

An appreciable number of other uranyl species are included in a relatively small number of the databases. This is particularly notable in the cases of the hydroxy–carbonate species – $(UO_2)_2(OH)_3CO_3^-$, $(UO_2)_3(OH)_3CO_3^+$, $(UO_2)_3(OH)_5CO_2^+$ and $(UO_2)_{11}(CO_3)_6(OH)_{12}^{2-}$, the alkaline earth metal–carbonate complexes $CaUO_2(CO_3)_3^{2-}$, $Ca_2UO_2(CO_3)_3^0$ and

299 $MgUO_2(CO_3)_3^{2-}$, the phosphate species $UO_2(H_2PO_4)_2^0$, $UO_2(H_2PO_4)_3^-$, $UO_2(H_2PO_4)(H_3PO_4)^+$
300 and $UO_2(H_2PO_4)_2^0$ the sulphate species $(UO_2)_2(OH)_2(SO_4)_2^{2-}$, $(UO_2)_3(OH)_4(SO_4)_4^{6-}$ and
301 $(UO_2)_4(OH)_7(SO_4)_4^{7-}$ and the silicate complex $UO_2H_3SiO_4^+$.

302 *4.2. Impacts of co–contaminants in scenarios*

303 Removing co–contaminants from model runs generally had negligible influence on the
304 predicted uranyl and thorium speciation. An exception was for the WHAM scenarios, where
305 removal of iron(III) from consideration was predicted to produce a shift in speciation from
306 uranyl adsorbed to colloidal HFO to uranyl complexed to other ligands. This is illustrated in
307 Figure 1, which shows predicted speciation for the Ritord scenario, using WHAM–m, under
308 conditions where (i) precipitated HFO has a chemically active surface, (ii) precipitated HFO
309 does not have a chemically active surface, (iii) iron(III) is absent. When HFO has a chemically
310 active surface, a small but non–negligible proportion (~9%) of the uranyl is predicted to be
311 adsorbed to HFO, with the major proportion (~85%) predicted to be bound to DOM and small
312 amounts present in free and hydrolysed forms (~2%) and carbonate complexes (~3%). If HFO
313 does not have a chemically active surface, binding to DOM is predicted to be higher (~93%)
314 with the amounts predicted to be free and hydrolysed (~3%) and as carbonate complexes (~4%)
315 slightly higher. If Fe(III) is absent then the prediction is for virtually all uranyl (>99%) to be
316 bound to DOM. Predicted free uranyl concentrations under these assumptions were 1.9×10^{-10} mol dm^{-3}, 2.1×10^{-10} mol dm^{-3} and 1.9×10^{-11} mol dm^{-3} respectively.

318 *4.3. Scope of model/database combinations for thorium speciation*

319 Table S1 in the Supplementary Information shows the binding constants for the inorganic
320 thorium solution species (complexes) in each model/database combination. The WHAM
321 database, which is identical in both the WHAM–d and WHAM–m situations, allows formation
322 of the monomeric thorium hydrolysis products $Th(OH)_n^{(4-n)+}$ (n = 1–4), the carbonate
323 complexes $ThCO_3^{2+}$ and $Th(CO_3)_5^{6-}$, the hydroxy–carbonate complexes $Th(OH)_2(CO_3)_3^{4-}$ and
324 $Th(OH)_3CO_3^-$, the sulphate complexes $Th(SO_4)_n^{(4-2n)+}$ (n = 1 to 3) and the halide complexes $ThCl^{3+}$,
325 ThF^{3+} and ThF_2^{2+}. As with uranyl, the databases for CHESS–ch, GWB–c and PHREEQC–l are
326 identical in respect of the thorium complexes that may form and their binding constants. The
327 databases all allow formation of the monomeric thorium hydrolysis products $Th(OH)_n^{(4-n)+}$
328 (n = 1–4), three polymeric hydrolysis products $Th_m(OH)_n^{(4m-n)+}$ with m = 2 and n = 2, m = 4 and
329 n = 8, m = 6 and n = 15. They also allow formation of a range of complexes with Cl^-, F^-, SO_4^{2-}
330 and PO_4^{3-} (see Table S1 for details). However, they have no binding constants for carbonate or
331 hydroxy–carbonate complex formation. VMIN–d and GWB–m also have similar databases,

albeit simulating formation of different complexes. Of the hydrolysis products, they simulate only $ThOH^{3+}$, $Th(OH)_2^{2+}$ and $Th_2(OH)_2^{6+}$, and of the carbonate and hydroxy–carbonate complexes only $Th(CO_3)_5^{6-}$ and $Th(OH)_3CO_3^-$. They also simulate $ThCl^{3+}$, ThF^{3+}, ThF_2^{2+}, ThF_3^+, ThF_4^0 and $ThNO_3^{3+}$, but have no constants for complexes with PO_4^{3-}. CHESS–ct simulates a similar range of complexes to CHESS–ch, also including $Th(CO_3)_5^{6-}$ and $Th(OH)_3CO_3^-$ but excluding any complexes with PO_4^{3-} except for the hydroxy–phosphate complex $Th(OH)_4PO_4^{3-}$, which is not found in any of the other databases. PHREEQC–m does not simulate any thorium complexes and so is not considered.

4.4. Predicted occurrence of major uranyl species

Default predictions for all scenarios in the absence of natural organic matter are shown in Figure 2.

In the Ritord scenario, WHAM–d and WHAM–m predicted that hydrolysis products and complexes containing carbonate would dominate when DOM/HFO were absent, comprising ~96% and ~97% of the uranyl respectively. Minor contributions from phosphate complexes (~2%) were predicted. WHAM–m, which allowed the formation of mixed hydroxy–carbonate complexes, predicted ~24% of uranyl to be present in this form. VMIN–d, which does not allow formation of hydroxy–carbonate complexes, also predicted that hydrolysis products (~20%) and carbonate complexes (~65%) would dominate, with a contribution from the silicate complex $UO_2H_3SiO_4^+$ (~14%). Predictions using CHESS–ch, GWB–c and PHREEQC–l were similar, as expected. Free and hydrolysed forms were predicted to dominate (~85%) with contributions from carbonate (~10–15%) and hydroxy–carbonate species (~1–3%). The CHESS–ct simulation predicted a much smaller contribution from free and hydrolysed species (~19%), with larger contributions from carbonate (~41%) and hydroxy–carbonate complexes (~39%). Inspection of the model outputs indicated that this was due to the standard log *K* for the $UO_2(OH)_2^0$ species being 1.44 greater in CHESS–ch, thus favouring formation of $UO_2(OH)_2^0$ in CHESS–ch at the expense of $UO_2CO_3^0$ and $(UO_2)_2CO_3(OH)_3^-$. Similar dominance of free and hydrolysed species was predicted by GWB–c and PHREEQC–l, as expected given that their databases are identical to that of CHESS–ch.

Similar differences were seen when comparing the simulations done using the Geochemist's Workbench. In the GWB–c simulation, free and hydrolysed species were predicted to dominate (~84%) with carbonate complexes also present (~15%). In the GWB–m simulation, carbonate complexes were predicted to dominate (~75%), with contributions from free and hydrolysed species (~12%), hydroxy–carbonate complexes (~6%) and the silicate complex $UO_2H_3SiO_4^+$

(~8%). The PHREEQC–l simulation predicted a dominance of free and hydrolysed species (~96%) with carbonate complexes (~3%) making up most of the remainder, while in the PHREEQC-m simulation the speciation was predicted to be made up largely of near equal contributions from carbonate complexes (~35%), free and hydrolysed species (~33%) and $UO_2H_3SiO_4^+$ (~29%).

In contrast to the Ritord results, the predicted speciation for the Beaverlodge scenario was consistently dominated by carbonate–containing complexes, regardless of the model or database used. Important differences among the predictions were still seen, particularly in respect to the predicted importance of the alkaline earth–uranyl-carbonate complexes. Where the database employed contained such ternary complexes, these were predicted to be dominant (~84% for WHAM–m, ~92% for Visual MINTEQ, ~97% for CHESS–ct, ~95% for GWB–m). In the remaining simulations carbonate complexes were predicted to dominate (~97–99%) with small amounts (~1–2%) present in the free ion and hydrolysed forms.

The simulations for Pit Lake also predicted dominance of alkaline earth–uranyl-carbonate complexes. In the four model/database combinations where they could form (WHAM–m, VMIN–d, CHESS–ct and GWB–m), they were predicted to make up at least 97% of the uranyl. In the CHESS–ch, GWB–c and PHREEQC–l scenarios, uranyl was predicted to be largely present as carbonate complexes split between free and hydrolysed forms (~14%), binary carbonate species (~43–44%) and mixed hydroxyl–carbonate species (~43%). Carbonate species were predicted to dominate in the WHAM–m and PHREEQC–m scenarios (~99–100%).

The Yellow Mountain scenario presented a more varied set of predictions than either Beaverlodge or Pit Lake. The WHAM–d scenario predicted dominance by carbonate complexes (>99%), while the WHAM–m scenario predicted that alkaline earth–carbonate complexes would dominate (~98%) with a minor contribution of carbonate complexes (~2%). VMIN–d predicted a dominance of alkaline earth–carbonates (~95%) with small contributions from carbonate complexes (~4%) and the free ion and hydrolysis products (~1%). The CHESS–ch and PHREEQC–l scenarios gave similar predictions, with the dominant species being free and hydrolysed forms (~39%) and hydroxy–carbonate species (~54–55%) with a small (~6%) contribution from carbonates. The CHESS–ct and GWB–m scenarios also predicted similar speciation, dominated by alkaline earth–carbonates (~76–81%) with contributions from hydroxy–carbonates (~15–17%) and carbonates (~3–6%). The PHREEQC–m scenario predicted carbonates (~64%) and free and hydrolysed forms (~36%) to dominate. The GWB–

c scenario predicted the free ion and hydrolysis products to dominate (~96%) with a small contribution from hydroxy–carbonate complexes (~3%).

For the Ritord scenario, predictions including DOM and colloidal HFO (Figure 3) presented a contrasts compared to those predictions obtained in the absence of DOM and HFO. WHAM–d predicted that uranyl bound to precipitated HFO was the dominant form (~58%), followed by uranyl bound to DOM (~40%), with small (<2% each) contributions from free and hydrolysed forms and carbonate complexes. In the WHAM–m scenario, predicted binding of uranyl to HFO was much reduced (~9%) while binding to DOM was predicted to be higher (~85%), with a small increase in the amounts predicted as the free ion and hydrolysed species, and as carbonate complexes. Addition of alkaline earth metal–carbonate and mixed hydroxy–carbonate complexes had a negligible effect on the predicted speciation. VMIN–d predicted that uranyl was almost entirely bound to organic matter, with minor contributions from free and hydrolysed forms, carbonate and silicate complexes. No adsorption to HFO was predicted, since strong complexation of Fe(III) by organic matter was predicted to prevent precipitation of HFO. In contrast, inclusion of DOM and colloidal HFO in the modelling of the remaining scenarios had only minor effects on the speciation. The Beaverlodge WHAM–d and WHAM–m predictions were similar to those made in the absence of DOM/HFO, with organic and HFO–bound species predicted to be <1%. VMIN–d predicted ~2% organically–complexed uranyl in Beaverlodge. Complexation to DOM and HFO in Pit Lake was negligible in all model/database combinations. In Yellow Mountain, VMIN–d predicted ~1% complexation to DOM, otherwise there were negligible differences compared to the predictions without DOM/HFO.

4.5. Predicted occurrence of major thorium species

As with uranyl, the predicted occurrence of thorium species across the different model/database combinations, in the absence of DOM and HFO, was variable. A notable pattern across the scenarios was the dominance of two specific complexes, $Th(OH)_4^0$ and $Th(OH)_3CO_3^-$. An important component of the variability of the predicted speciation was determined by whether the database used contained binding constants for these complexes. In Beaverlodge, WHAM–d/WHAM–m predicted that $Th(OH)_4^0$ dominated (~79%) with a major contribution from $Th(OH)_3CO_3^-$ (~21%). In the VMIN–d and GWB–m model/database combinations, for which the binding constant for $Th(OH)_4^0$ was absent, $Th(OH)_3CO_3^-$ completely dominated speciation (~100%). Conversely, CHESS–ch, GWB–c and PHREEQC–l, for which the binding constant for $Th(OH)_3CO_3^-$ was absent, predicted ~100% $Th(OH)_4^0$. CHESS–ct, which has binding constants for both $Th(OH)_4^0$ and $Th(OH)_3CO_3^-$, predicted complete dominance of $Th(OH)_4^0$.

Patterns of prediction for VMIN–d, GWB–m, CHESS–ch, GWB–c and PHREEQC–l in the Pit Lake and Yellow Mountain scenarios were similar to their predictions in the Beaverlodge scenario. WHAM–d and WHAM–m predicted dominance of $Th(OH)_4^0$ and $Th(OH)_3CO_3^-$ in Pit Lake and Yellow Mountain, with differing degrees of importance (~23% and ~77% in Pit Lake, ~52% and ~48% in Yellow Mountain). CHESS–ct predicted thorium to be largely present as $Th(OH)_4^0$ (~99% in Pit Lake and ~95% in Yellow Mountain) with the remainder being $Th(OH)_4^0$.

When including DOM/HFO in the WHAM–d, WHAM–m and VMIN–d predictions, contrasting patterns were found. WHAM predicted that DOM–bound thorium was a minor component in all the scenarios (~2% in Beaverlodge and <1% in both Pit Lake and Yellow Mountain). In contrast, VMIN–d consistently predicted complete dominance (~100%) of DOM–complexed thorium in all three scenarios. The contribution of HFO–bound thorium was consistently negligible in all predictions.

5. Discussion

Dissolved uranyl and thorium speciation is somewhat complex in comparison with other metallic cations due to the possibility of forming a relatively large number of hydrolysis products (including small polymeric species) and complexes with inorganic ligands, particularly carbonate, at environmentally relevant concentrations. This is coupled with the possibility of forming mixed complexes containing either another metal centre (alkali metal–carbonate complexes, in the case of uranyl) or two ligand types (e.g. hydroxy–carbonate complexes).

In general the effects of co-contaminants on predicted uranyl and thorium speciation were negligible. The exception is the WHAM7 simulation for Ritord where Fe is considered as a co–contaminant. Here, inclusion of Fe (as Fe(III)) in the simulation inputs results in the prediction of precipitation of HFO and adsorption of uranyl to the HFO surface. Simulation preventing adsorption to HFO predicts speciation to be dominated by DOM complexes, with a higher predicted UO_2^{2+} activity due to the lower ligand concentration. Simulation with Fe(III) absent, on the other hand, predicts the greatest extent of complexation (almost entirely to DOM) and the lowest UO_2^{2+} activity, due to the removal of Fe(III) as a competing ion for uranyl binding to DOM. A predicted difference in the free uranyl activity of approximately one order of magnitude was seen between the scenarios where Fe(III) was present and absent. However, since freshwaters are frequently oversaturated with respect to HFO (e.g. Lofts and

Tipping, 2008) and Fe(III) is thus under solid phase control, the competitive effect of Fe^{3+} ions on complexation of cations is ubiquitous whether Fe(III) is present as a co–contaminant or not. It is possible that uranyl binding to HFO may be important in pyritic acid mine drainage systems, where oxidation of high concentrations of Fe(II) produced by pyrite dissolution can produce elevated concentrations of HFO which may exert a significant control on metal speciation and transport (e.g. Balistrieri et al., 2007).

The effect of Fe(III) was negligible in the other scenarios, due to its relatively low concentrations (Table 2) and the higher hardness and/or pH, which increased uranyl–carbonate association. This limited the formation of HFO and thus of uranyl–HFO adsorbed complexes. Formation of uranyl adsorbed to HFO did not exceed ~1% of total uranyl in the other scenarios.

The considerable variations in predicted speciation for each scenario across the different model/database combinations illustrate how differences among the databases clearly influence the computed speciation. Complexation of uranyl to DOM is predicted to be of importance in scenarios where the DOM:carbonate ratio is sufficiently high to allow DOM to effectively compete with carbonate for uranyl, such as in the Ritord scenario. In the Beaverlodge scenario, almost complete formation of simple carbonate complexes is predicted if formation of alkaline earth–carbonate complexes is not allowed, whereas alkaline earth–carbonate complexes dominate if they can form. A similar pattern is seen in the Pit Lake and Yellow Mountain scenarios: if neither alkaline earth–carbonate complexes nor hydroxy–carbonate complexes may form, simple carbonates are predicted to dominate; if hydroxy–carbonate complexes may form, but not alkaline earth–carbonate complexes, then hydroxy–carbonate complexes are important, but if alkaline earth–carbonate complexes can form then they dominate. The patterns observed in the thorium predictions are simpler and dominated by $Th(OH)_4^0$ and $Th(OH)_3CO_3^-$; for specific model/database combinations, the predicted speciation is highly dependent on whether either or both of these complexes are allowed to form. Simulations involving DOM/HFO showed contrasting predicted binding behaviour of thorium between WHAM and Visual MINTEQ, with the latter predicting that DOM complexes completely dominated thorium speciation, while the former predicted them to be of minor importance. Further work is clearly needed to better quantify the actual importance of DOM for uranyl and thorium complexation in surface waters, to provide data against which to further assess and improve the models and to constrain their predictions. Coupled with this, there needs to be a raising of awareness among users of geochemical speciation modelling, regarding the importance of assessing database coverage and completeness prior to performing computations.

As noted in the introduction, a further intention of this study was to model radium and polonium alongside uranium and thorium, but this was not possible due to a general lack of binding constants in the model databases. This is a notable data gap given the importance of radium as a decay product of uranium and thorium. Some work on estimating Ra^{2+} binding constants exists; Langmuir and Riese (1985) estimated binding constants and enthalpies for some simple Ra^{2+} complexes ($RaOH^+$, $RaCO_3^0$, $RaCl^+$, $RaSO_4^0$) by extrapolation from the relationship between the corresponding binding constants for other Group II metals (Ca, Sr, Ba) and the effective ionic radius of the cation. However, such estimated constants for solution complexes are not generally incorporated into speciation modelling databases. While no literature studies on the binding of radium to humic substances could be identified, in this case the estimation of binding constants is possible in principle (e.g. Tipping et al., 2011). In order to incorporate radium complex formation into speciation model databases, experimental research is required on the solution complexation of radium, and ideally also on its interactions with humic substances.

6. Conclusions

- Well–characterised field waters, with minor extrapolation where required, were used to compare geochemical model predictions of dissolved uranyl (in four scenarios) and thorium speciation (in three scenarios) and to investigate the influence of co–contaminants on the predicted forms of uranyl and thorium.
- Removal of co–contaminants from simulations generally had negligible effects on the predicted speciation, with the exception of the Ritord scenario where simulation using WHAM7 in the absence of iron prevented formation of uranyl adsorbed to HFO. This suggests iron could have a significant influence on uranyl speciation in waters receiving iron–rich inputs such as acid mine drainage.
- Speciation predictions were dependent on model capabilities and the coverage of inorganic and organic complexes in the database used.
- Organic complexation, where it could be simulated, was predicted to be important for uranyl in a slightly acidic water of relatively high DOM concentration. Binding of thorium to DOM was predicted to dominate speciation in circumneutral waters when modelled using Visual MINTEQ, however predictions of the same waters using WHAM7 predicted only a minor role for DOM in binding thorium.

- Thorium speciation was predicted to be controlled by a small number of specific complexes. Variations in predicted speciation were strongly dependent on the presence/absence of these complexes from the database used.
- In circumneutral waters, formation of carbonate complexes, including hydroxy–carbonates and alkaline earth metal–carbonates, was predicted to dominate the uranyl speciation.
- Differences in the range of carbonate complexes considered in the model databases had an important influence on uranyl speciation predictions in circumneutral waters, where inorganic complexes were predicted to dominate. Alkaline earth metal–carbonate and hydroxy–carbonate complexes were predicted to be important species in such waters, when they were included in simulations. Where they were absent, simple carbonate species were generally predicted to be important.
- Complexation constants for radium and polonium were entirely absent from all the databases and so no assessment of speciation was possible. There is a need for experimental determination of radium and polonium complexation constants in order to properly incorporate these elements into geochemical speciation models.
- Model users need to be aware of the differences among model databases before applying models, in particular the status with respect to updates and the incorporation of the most up to date binding constants.

Acknowledgements

This research was done within the STAR (A STrategy for Allied Radioecology) Network of Excellence supported by the EC-EURATOM 7th Framework Programme (Contract Number: Fission-2010-3.5.1-269672).

References

Amme, M., 2002. Geochemical modelling as a tool for actinide speciation during anoxic leaching processes of nuclear fuel. Aquatic Geochemistry 8: 177–198.

Balistrieri, L.S., Seal, R.R., Piatak, N.M., Paul, B., 2007. Assessing the concentration, speciation, and toxicity of dissolved metals during mixing of acid–mine drainage and ambient river water downstream of the Elizabeth Copper Mine, Vermont, USA. Applied Geochemistry 22: 930–952.

Benedetti, M.F., Milne, C.J., Kinniburgh, D.G., Van Riemsdijk, W.H., Koopal, L.K., 1995. Metal–ion binding to humic substances – application of the nonideal competitive adsorption model. Environmental Science and Technology 29: 446–457.

Bethke, C.M., Yeakel, S., 2012. The Geochemists Workbench® Version 9.0: GWB Essentials Guide. Aqueous Solutions, LLC, Champaign, IL, U.S.A.

Cameco Corp., 2011. Beaverlodge Project Annual Report, Year 25 – Transition Phase Period January 1, 2010 to June 30, 2011. Saskatoon, Sask., Canada.

Denison, F.H., 2004. Uranium(VI) speciation: modelling, uncertainty and relevance to bioavailability models. Application to uranium uptake by the gills of a freshwater bivalve. University Aix-Marseille I, ,Biosciences de l'Environnement, Chimie et Santé, PhD thesis, 347pp.

Denison, F.H., Garnier-Laplace, J., 2005. The effects of database parameter uncertainty on uranium(VI) equilibrium calculations. Geochimica et Cosmochimica Acta 69: 2183–2191.

Dong, W., Brooks, S.C., 2006. Determination of the formation constants of ternary complexes of uranyl and carbonate with alkaline earth metals (Mg^{2+}, Ca^{2+}, Sr^{2+}, and Ba^{2+}) using anion exchange method. Environmental Science & Technology 40: 4689–4695.

Dzombak, D.A., Morel, F.M.M., 1990. Surface Complexation Modeling: Hydrous Ferric Oxide. John Wiley & Sons, New York.

Farley, K.J., Meyer, J.S., Balistrieri, L.S., De Schamphelaere, K.A.C., Iwasaki, Y., Janssen, C.R., Kamo, M., Lofts, S., Mebane, C.A., Naito, W., Ryan, A.C., Santore, R.C., Tipping, E., 2014. Metal Mixture Modeling Evaluation project: 2. Comparison of four modeling approaches. Environmental Toxicology and Chemistry, DOI: 10.1002/etc.2820.

Fortin, C., Dutel L., Garnier-Laplace J., 2004. Uranium complexation and uptake by a green algae in relation to chemical speciation: the importance of the free uranyl ion. Environmental Toxicology and Chemistry 23: 974–981.

Fortin, C, Denison, F.H, Garnier-Laplace, J., 2007. Metal–phytoplankton interactions: Modeling the effect of competing ions (H^{+}, Ca^{2+}, and Mg^{2+}) on uranium uptake. Environmental Toxicology and Chemistry 26: 242–248.

Franklin, N.M., Stauber, J.L., Markich, S.J., Lim, R.P., 2000. pH–dependent toxicity of copper and uranium to a tropical freshwater alga (*Chlorella* sp.). Aquatic Toxicology 48: 275–289.

588 Garnier–Laplace, J., Beaugelin–Seiller, K., Gilbin, R., Della–Vedova, C., Jolliet, O., Payet,
589 J., 2009. A Screening Level Ecological Risk Assessment and ranking method for liquid
590 radioactive and chemical mixtures released by nuclear facilities under normal operating
591 conditions. Radioprotection 44: 903–908.

592 Geipel, G., Amayri, S., Bernhard, G., 2008. Mixed complexes of alkaline earth uranyl
593 carbonates: A laser–induced time–resolved fluorescence spectroscopic study. Spectrochimica
594 Acta Part A–Molecular and Biomolecular Spectroscopy 71: 53–58.

595 Grenthe, I., Fuger, J., Konings, R.J.M., Lemire, R.J., Muller, A. B., Nguyen–Trung Cregu,
596 C., Wanner, H. 2004., Chemical Thermodynamics of Uranium. Nuclear Energy Agency,
597 Organisation for Economic Co–operation and Development, Paris, France.

598 Hegazy, A.K., Afifi, S.Y., Alatar, A.A., Alwathnani, H.A., Emam, M.H., 2013. Soil
599 characteristics influence the radionuclide uptake of different plant species. Chemistry and
600 Ecology 29: 255–269.

601 Herlory, O., Bonzom, J.M., Gilbin, R., Frelon, S., Fayolle, S., Delmas, F., Coste, M., 2013.
602 Use of diatom assemblages as biomonitor of the impact of treated uranium mining effluent
603 discharge on a stream: Case study of the Ritord watershed (Center-West France).
604 Ecotoxicology 22: 1186–1199.

605 Hydrogeologic, Inc, & Allison Geoscience Consultants, Inc., 1999.
606 MINTEQA2/PRODEFA2, a geochemical assessment model for environmental systems,
607 Version 4.0 Users Manual. U.S. Environmental Protection Agency, Athens, GA, U.S.A.

608 Jho, E.H., An, J., Nam, K., 2011. Extended biotic ligand model for prediction of mixture
609 toxicity of Cd and Pb using single metal toxicity data. Environmental Toxicology and
610 Chemistry 30: 1697–1703.

611 KHS Environmental Management Group Ltd., 2004. Beaverlodge Mine – Mill
612 Decommissioning Annual Report (Year 19 – Transition Phase). Period: July 1, 2003 – June
613 30, 2004. Domremy, Sask., Canada.

614 Langmuir, D., Riese, A.C., 1985. The thermodynamic properties of radium. Geochimica et
615 Cosmochimica Acta 49: 1593–1601.

616 Lavoie, M., Sabatier, S., Garnier-Laplace, J., Fortin C., 2014. Uranium accumulation and
617 toxicity in the green algae *Chlamydomonas reinhardtii* is modulated by pH. Environmental
618 Toxicology and Chemistry 33: 1372–1379.

619 Liu, D.J., Bruggeman, C., Maes, N., 2008. The influence of natural organic matter on the
620 speciation and solubility of Eu in Boom Clay porewater. Radiochimica Acta 96: 711-720

621 Lofts, S., Tipping, E., 1998. An assemblage model for cation binding by natural particulate
622 matter. Geochimica et Cosmochimica Acta 62: 2609–2625.

623 Lofts, S., Tipping, E., 2008. The Chemical Speciation of Fe(III) in Freshwaters. Aquatic
624 Geochemistry 14: 337–358.

625 Lofts, S., Tipping, E., 2011. Assessing WHAM/Model VII against field measurements of free
626 metal ion concentrations: model performance and the role of uncertainty in parameters and
627 inputs. Environmental Chemistry 8: 501–516.

628 Mahoney, J.J., Cadle, S.A., Jakubowski, R.T., 2009. Uranyl Adsorption onto Hydrous Ferric
629 Oxide—A Re-Evaluation for the Diffuse Layer Model Database. Environmental Science &
630 Technology 43: 9260–9266.

631 Maher K., Bargar J.R., Brown G.E., 2013. Environmental Speciation of Actinides. Inorganic
632 Chemistry 52: 3510–3532.

633 Markich, S.J., 2013. Water hardness reduces the accumulation and toxicity of uranium in a
634 freshwater macrophyte (*Ceratophyllum demersum*). Science of The Total Environment 443:
635 582 –589.

636 Marsac, R., Davranche, M., Gruau, G., Bouhnik-Le Coz, M., Dia, A., 2011. An improved
637 description of the interactions between rare earth elements and humic acids by modeling:
638 PHREEQC-Model VI coupling, Geochimica et Cosmochimica Acta 75: 5625-5637

639 Meyer, J.S., 2002. The utility of the terms “bioavailability” and “bioavailable fraction” for
640 metals, Marine Environmental Research 53: 417–423.

641 Moulin, V., Tits, J., Ouzounian, G., 1992. Actinide speciation in the presence of humic
642 substances in natural–water conditions. Radiochimica Acta 58–9: 179–190.

643 Nash K.L., Choppin, G.R., 1980. Interaction of humic and fulvic acids with Th(IV). Journal
644 of Inorganic and Nuclear Chemistry 42: 1045–1050.

645 O'Loughlin, E.J., Boyanov, M.I., Antonopoulos, D.A., Kemner, K.M., 2011. Redox Processes
646 Affecting the Speciation of Technetium, Uranium, Neptunium, and Plutonium in Aquatic and
647 Terrestrial Environments. In Tratnyek PG, Grundl TJ, Haderlein SB, eds, Aquatic Redox
648 Chemistry. Vol 1071-ACS Symposium Series, pp 477–517.

649 Paquin, P.R., Gorsuch, J.W., Apte, S., Batley, G.E., Bowles, K.C., Campbell, P.G.C., Delos,
650 C.G., Di Toro, D.M., Dwyer, R.L., Galvez, F., Gensemer, R.W., Goss, G.G., Hogstrand ,C.,
651 Janssen, C.R., McGeer, J.C., Naddy, R.B., Playle, R.C., Santore, R.C., Schneider, U.,
652 Stubblefield, W.A., Wood, C.M., Wu, K.B. 2002., The biotic ligand model: a historical
653 overview. Comparative Biochemistry and Physiology C-Toxicology and Pharmacology 133:
654 3–35.

655 Rojo, I., Seco, F., Rovira, M., Giménez, J., Cervantes, G., Martí, V., de Pablo, J., 2009.
656 Thorium sorption onto magnetite and ferrihydrite in acidic conditions. Journal of Nuclear
657 Materials 385: 474–478.

658 Saito, T., Nagasaki, S., Tanaka, S., Koopal, L.K., 2004. Application of the NICA-Donnan
659 model for proton, copper and uranyl binding to humic acid. Radiochimica Acta 92: 567–574.

660 Skipperud, L., Strømman, G., Yunusov, M., Stegnar, P., Uralbekov, B., Tilloboev, H.,
661 Zjazjev, G., Heier, L.S., Rosseland, B.O., Salbu, B., 2013. Environmental impact assessment
662 of radionuclide and metal contamination at the former U sites Taboshar and Digmai,
663 Tajikistan. Journal of Environmental Radioactivity 123: 50–62.

664 Smith, R.M., Martell, A.E., Motekaitis, R.J., 2003. NIST Critically Selected Stability
665 Constants of Metal Complexes Database. NIST Standard Reference Database 46, version 7.0.
666 NIST, Gaithersburg, MD, USA.

667 Tipping, E., 1994. WHAM – a chemical–equilibrium model and computer code for waters,
668 sediments, and soils incorporating a discrete site electrostatic model of ion-binding by humic
669 substances. Computers and Geosciences 20: 973–1023.

670 Tipping, E., Lofts, S., Sonke, J.E., 2011. Humic Ion-Binding Model VII: a revised
671 parameterisation of cation-binding by humic substances. Environmental Chemistry 8: 225–
672 235.

673 Trenfield, M.A., McDonald, S., Kovacs, K., Lesher, E.K., Pringle, J.M., Markich, S.J., Ng,
674 J.C., Noller, B., Brown, P.L., van Dam, R.A., 2011a. Dissolved Organic Carbon Reduces
675 Uranium Bioavailability and Toxicity. 1. Characterization of an Aquatic Fulvic Acid and Its
676 Complexation with Uranium[VI]. Environmental Science and Technology 45: 3075–3081.

677 Trenfield, M.A., Ng, J.C., Noller, B.N., Markich, S.J., van Dam, R.A., 2011b. Dissolved
678 Organic Carbon Reduces Uranium Bioavailability and Toxicity. 2. Uranium[VI] Speciation
679 and Toxicity to Three Tropical Freshwater Organisms. Environmental Science and Technology
680 45: 3082–3089.

Van der Lee, J., 1998. Thermodynamic and mathematical concepts of CHESS. Ecole desMines de Paris, Paris.

Van der Lee, J., Lomenech, C., 2004. Towards a common thermodynamic database for speciation models. Radiochimica Acta 92: 811–818.

Vanhoudt, N., Vandenhove, H., Real, A., Bradshaw C., Stark K., 2012. A review of multiple stressor studies that include ionising radiation. Environmental Pollution 168:177-192.

Vercouter, T., Reiller, P.E., Ansoborlo, E., Février, L., Gilbin, R., Lomenech, C., Philippini, V., 2015. A modelling exercise on the importance of ternary alkaline earth carbonate species of uranium(VI) in the inorganic speciation of natural waters. Applied Geochemistry. DOI:10.1016/j.apgeochem.2014.11.016

Vitorge, P., Capdevila, H., 2003. Thermodynamic data for modelling actinide speciation in environmental waters. Radiochimica Acta 91:623–631.

Waite, T.D., Davis, J.A., Payne, T.E., Waychunas, G.A., Xu, N., 1994. Uranium(VI) adsorption to ferrihydrite: Application of a surface complexation model. Geochimica et Cosmochimica Acta 58: 5465–5478.

Zeman, F., Gilbin, R., Alonzo, F., Lecomte-Pradines, C., Garnier-Laplace, J., Aliaume, C., 2008. Effects of waterborne uranium on survival, growth, reproduction and physiological processes of the freshwater cladoceran Daphnia magna. AquaticToxicology 86(3): 370–378.

699

700 Table 1. Major ion concentrations in scenario waters. nm = not measured.

	Determinant														
	pH	DOC mg dm^{-3}	Na mg dm^{-3}	Mg mg dm^{-3}	Al mg dm^{-3}	K mg dm^{-3}	Ca mg dm^{-3}	NH_4 mg dm^{-3}	Cl mg dm^{-3}	NO_3 mg dm^{-3}	SO_4 mg dm^{-3}	HCO_3 mg C dm^{-3} [a]	Alk mg $CaCO_3$ dm^{-3}	F mg dm^{-3}	Si mg dm^{-3}
Ritord	6.38	9.57	6.2	3.1	0.205	2.7	17.4	0.22	14.4	1.7	48	1.97	nm	nm	12.17
Beaverlodge [b]	8.05 [b]	14.0 [c]	54.7 [b]	5.2 [b]	nm	1.5 [b]	25.2 [b]	nm	6.64 [b]	nm	50.6 [b]	169.7 [b]	nm	nm	nm
Pit Lake	8.0	2.23	111	36	nm	3.6	126	nm	14	0.15	471	nm	207 [e]	0.37	nm
Yellow Mountain	7.4	0.78	89	28	nm	3.3	157	nm	14	5	399	nm	258 [e]	0.45	nm

701 [a] mg inorganic carbon dm^{-3}.

702 [b] n = 11.

703 [c] n = 1.

704 [d] mg inorganic C dm^{-3}.

705 [e] Estimated using WHAM7, assuming ionic charge difference to be due to carbonate species.

706

707 Table 2. Trace metal, metalloid, uranium and thorium concentrations in scenario waters. nm = not measured.

	Determinand											
	As	Cu	Mn	Fe	Ni	Zn	Se	Mo	Ba	Pb	U	Th
	µg dm^{-3}	µg dm^{-3}	µg dm^{-3}	µg dm^{-3}	µg dm^{-3}	µg dm^{-3}	µg dm^{-3}	µg dm^{-3}	µg dm^{-3}	µg dm^{-3}	µg dm^{-3}	pg dm^{-3}
Ritord	nm	nm	307	721	nm	nm	nm	nm	241	nm	35	nm
Beaverlodge	1.8 [a]	1 [b]	nm	65 [b]	1 [b]	5 [b]	4.8 [c]	nm	0.56 [d]	3 [b]	483.6	0.079
Pit Lake	25	nm	13	18	3.8	(65)[e]	nm	34	nm	0.37	2000	4989
Yellow Mountain	31	nm	1	13	4.8	(65)[e]	nm	15	nm	0.3	1100	499

708 [a] $n = 2$.

709 [b] $n = 4$.

710 [c] $n = 7$.

711 [d] $n = 9$.

712 [e] Estimated at 10^{-6} mol dm^{-3}.

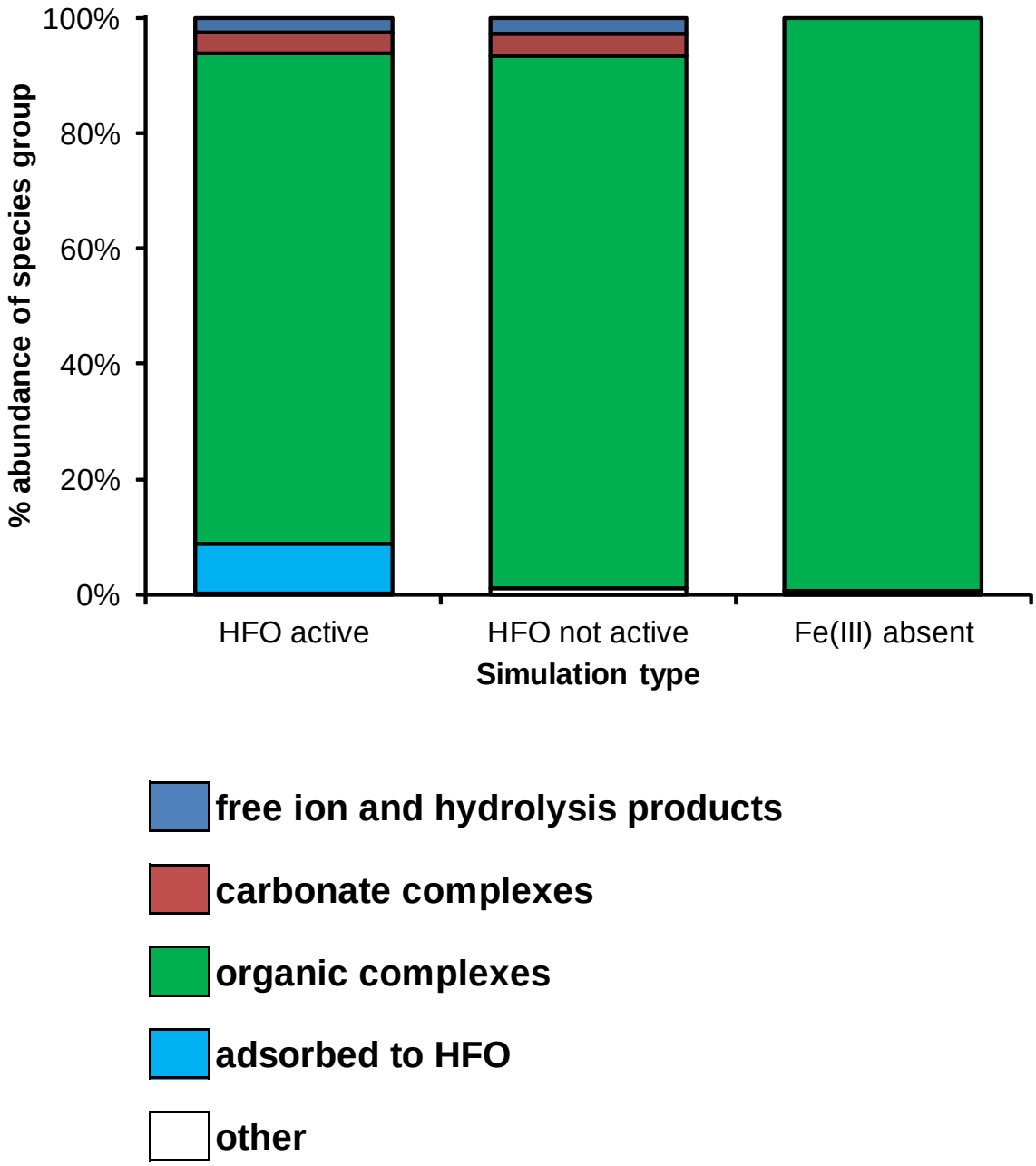

713

714 Figure 1.

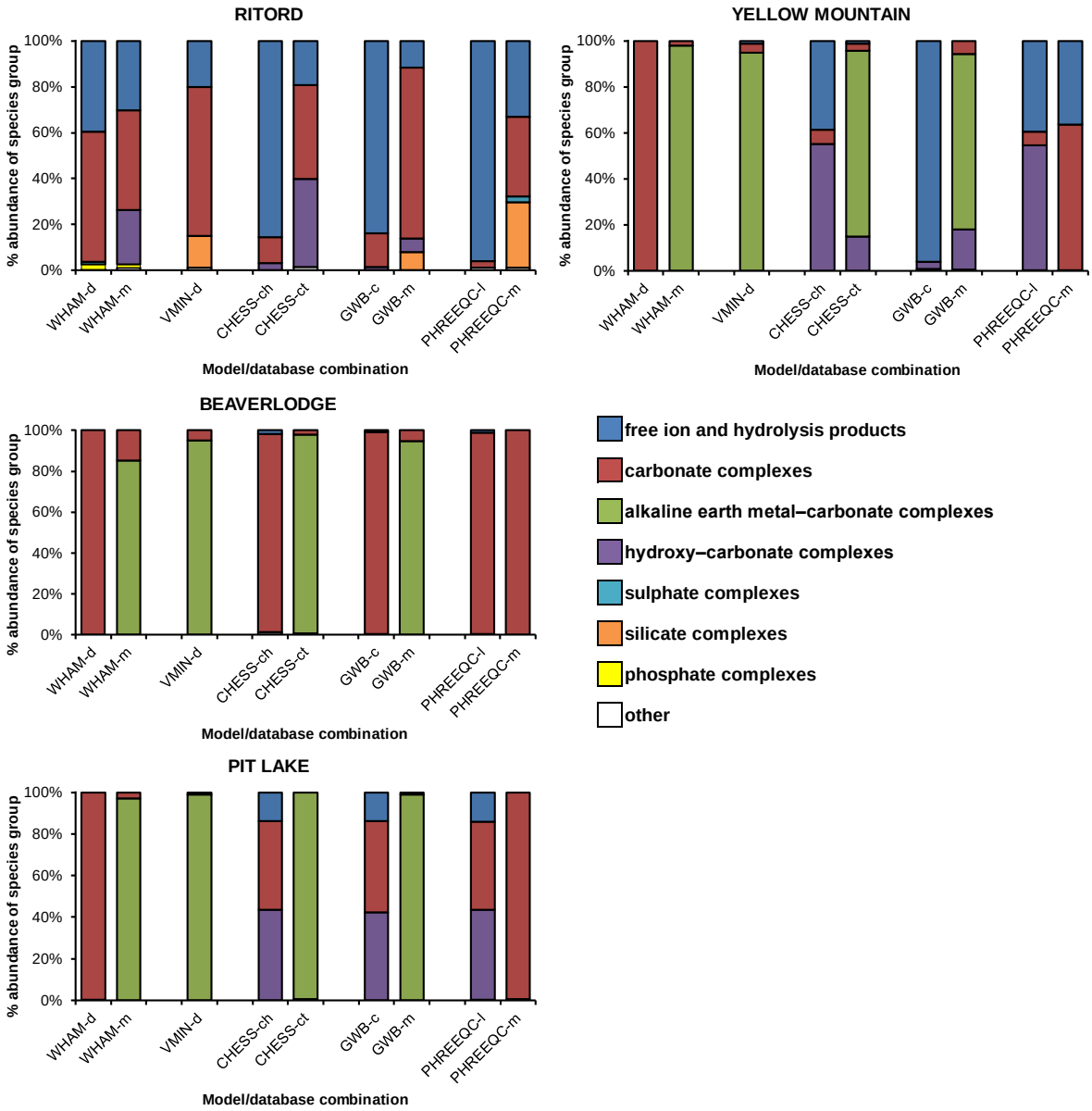

715

716 Figure 2.

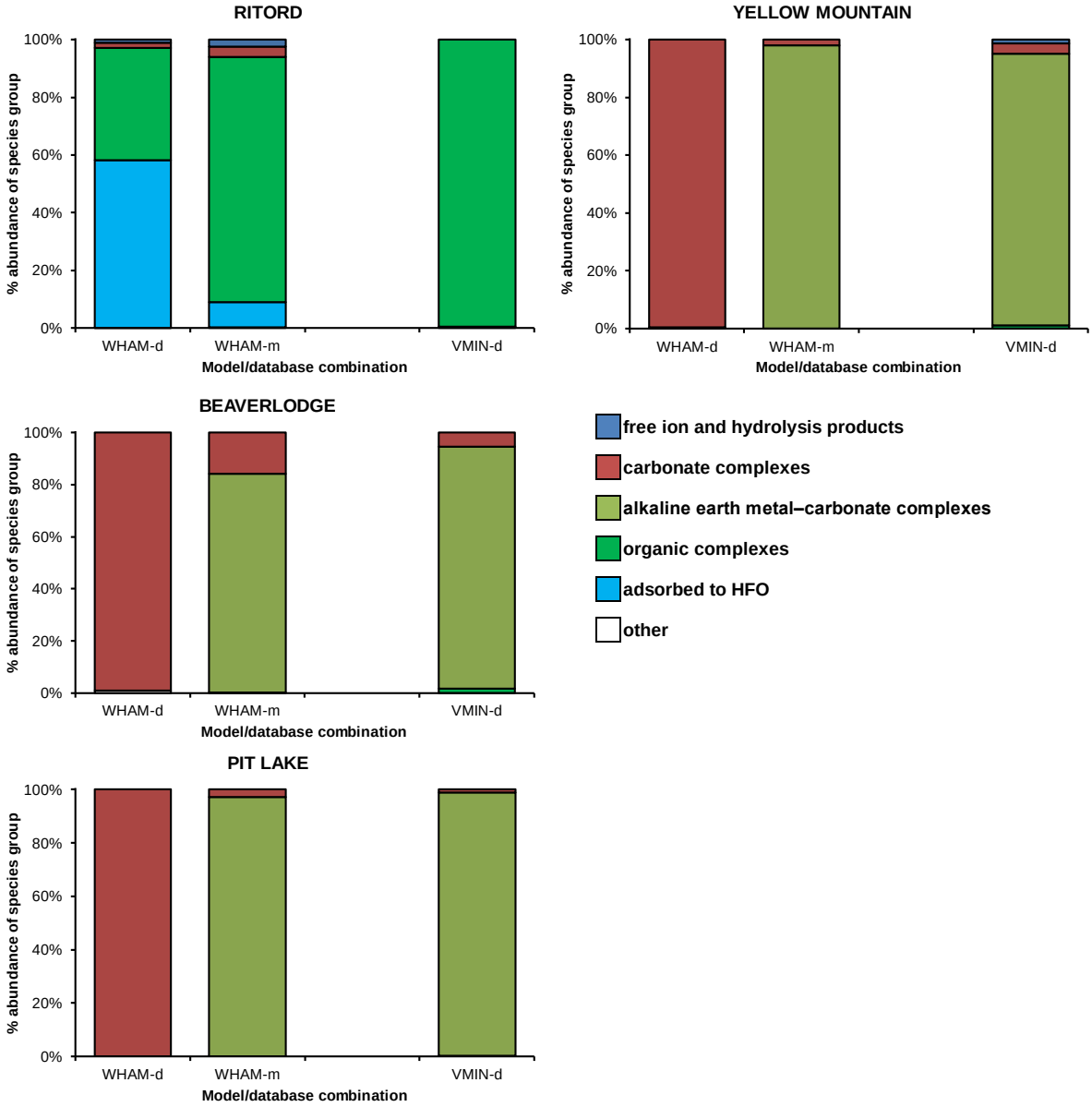
RITORD
YELLOW MOUNTAIN
BEAVERLODGE
PIT LAKE
% abundance of species group
100%
80%
60%
40%
20%
0%
WHAM-d
WHAM-m
VMIN-d
Model/database combination
free ion and hydrolysis products
carbonate complexes
alkaline earth metal–carbonate complexes
organic complexes
adsorbed to HFO
other

Figure 3.

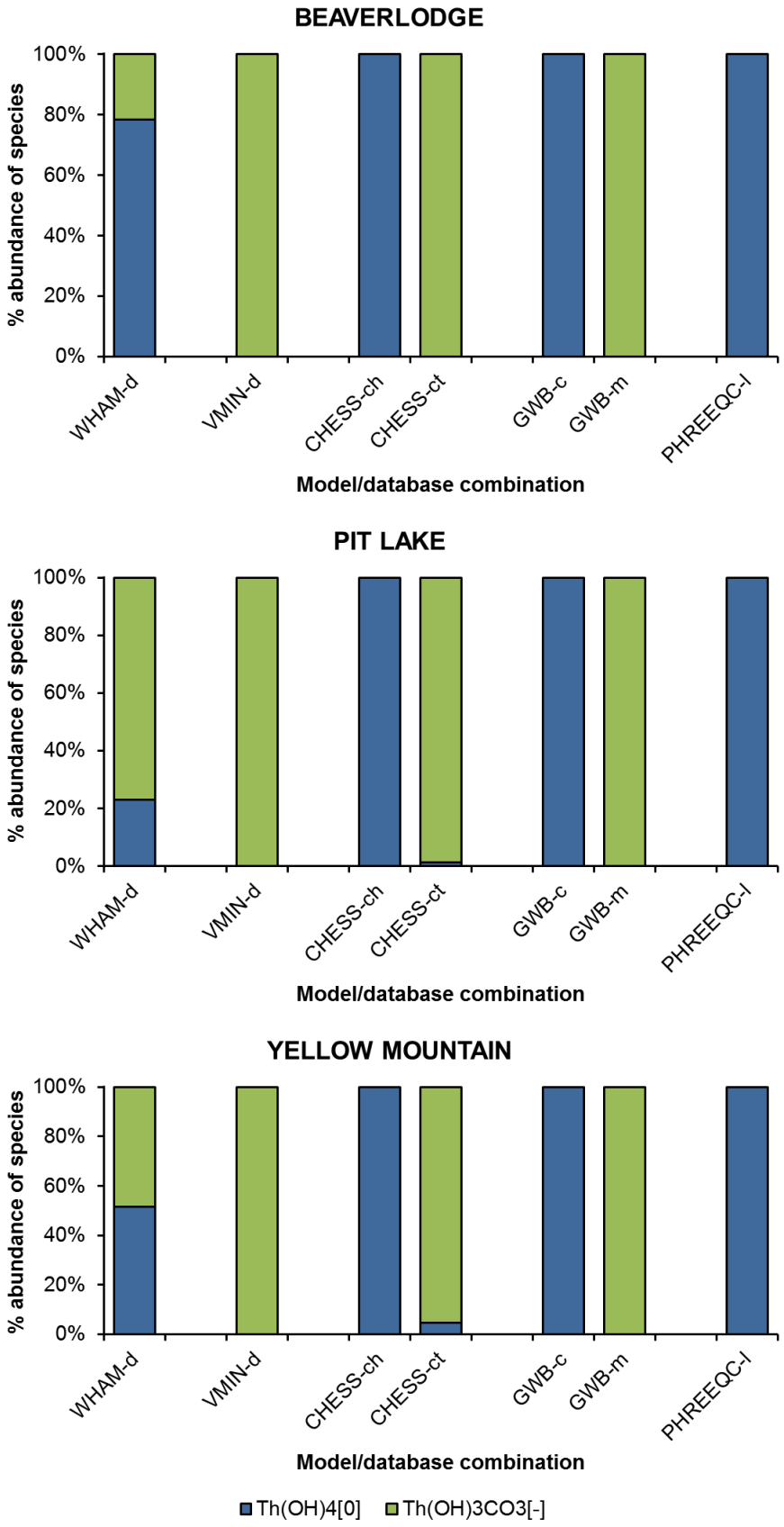

720

721 Figure 4.

Figure captions

Figure 1. Predictions of speciation in the Ritord scenario using WHAM–m, under three assumptions: Fe(III) present and able to form HFO with a chemically active surface; Fe(III) present but not allowed to form HFO; Fe(III) not present.

Figure 2. Predicted distribution of uranyl among groups of complexes for each model/database combination, in the absence of natural organic matter and colloidal HFO. Charts show the distribution of uranyl among defined groups of species: the free ion and its hydrolysis products, carbonate complexes, alkaline earth metal–carbonate complexes, hydroxy–carbonate complexes, sulphate complexes, silicate complexes and phosphate complexes. Species groups whose occurrence represent <1% of the uranyl in a given calculation are shown under 'Other'. Mixed hydroxy–carbonate complexes can form only in the CHESS–ch, CHESS–ct, GWB–c and GWM–m simulations. Silicate complexation can only be simulated where Si measurements were made (Ritord scenario) and in the VMIN–d, GWB–m and PHREEQC–m simulations.

Figure 3. Predicted distribution of uranyl among groups of complexes for the model/database combinations WHAM–d, WHAM–m and VMIN–d, in the presence of natural organic matter and allowing colloidal HFO to form.

Figure 4. Predicted distribution of thorium among complexes for each model/database combination, in the absence of natural organic matter and colloidal HFO. Only the dominant species $Th(OH)_4^0$ and $Th(OH)_3CO_3^-$ are shown. The complex $Th(OH)_4^0$ can form in the WHAM–d, CHESS–ch, CHESS–ct, GWB–c and PHREEQC–l simulations. The complex $Th(OH)_3CO_3^-$ can form in the WHAM–d, VMIN–d, CHESS–ct and GWB–m simulations.

Supplementary Information

Assessment of co–contaminant effects on uranium and thorium speciation in freshwater using geochemical modelling

Stephen LOFTS[a], Laureline FEVRIER[b], Nele HOREMANS[c], Rodolphe GILBIN[b], Christophe BRUGGEMAN[c], Hildegarde VANDENHOVE[c]

[a] NERC Centre for Ecology and Hydrology, Lancaster Environment Centre, Bailrigg, Lancaster, LA1 4AP, U.K.. stlo@ceh.ac.uk

[b] IRSN, DEI/SECRE/LRE-Bât 186, B.P.3, Cadarache Center, F-13115 Saint-Paul-lez-Durance cedex, France. laureline.fevrier@irsn.fr, rodolphe.gilbin@irsn.fr

[c] Belgian Nuclear Research Centre SCK•CEN, BE-2400 Mol, Belgium. nhoreman@sckcen.be, cbruggeman@scksen.be, hvandenhove@sckcen.be

Corresponding author: S. Lofts

1. Summary of binding complexes

Table S1. Thermodynamic data[a,b,c,d] for solution complexes of uranyl and thorium simulated by each model/database combination. Reaction enthalpies for the CHESS–ch/GWB–c and CHESS–ct databases are computed by interpolation of point log *K* values for 0ºC and 25ºC using the Van't Hoff equation. Underlining denotes where the value in the database is the same as that in the NEA-TDB compilation (Guillaumont et al., 2003).

Model/database combination	WHAM-d[a,b]		WHAM-m[a,b]		VMIN-d, GWB-m		CHESS-ch[c,d], GWB-c[c,d]		CHESS-ct[c,d]		PHREEQC-l[c,d]		PHREEQC-m[b]	
Database name	default		modified		v3.0, thermo.minteq		chess.tdb, thermo.com.v8.r6+		ctdpv3_Dong.tdb		llnl		minteq	
Complex	log *K*, 25ºC	ΔH, kJ/mol	log *K*, 25ºC	ΔH, kJ/mol	log *K*, 25ºC	ΔH, kJ/mol	log *K*, 25ºC	ΔH, kJ/mol	log *K*, 25ºC	ΔH, kJ/mol	log *K*, 25ºC	ΔH, kJ/mol	log *K*, 25ºC	ΔH, kJ/mol
UO_2OH^+	-5.2	**44.94**	-5.2	**44.94**	-5.25	[e]	-5.2073	**43.7**	-5.36	**42.8**	-5.2073	**41.2**	-5.09	
$UO_2(OH)_2^0$	-11.9		-11.9		-12.15		-10.3146		-11.75		-10.3146			
$UO_2(OH)_3^-$	-21		-21		-20.25		-19.2218		-19.6		-19.2218			
$UO_2(OH)_4^{2-}$	-32.4	**156.3**	-32.4	**156.3**	-32.4		-33.0291		-34.23		-33.0291			
$(UO_2)_2OH^{3+}$					-2.7		-2.7072		-2.7		-2.7072			
$(UO_2)_2(OH)_2^{2+}$	-5.6	**40.1**	-5.6	**40.1**	-5.62	**48.9**	-5.6346	**39.8**	-5.7		-5.6346	**37.6**	-5.645	
$(UO_2)_3(OH)_4^{2+}$					-11.9		-11.929		-11.9		-11.929			
$(UO_2)_3(OH)_5^+$	-15.7	**100.4**	-15.7	**100.4**	-15.55	**123**	-15.5862	**102.0**	-15.59		-15.5862	**97.1**	-15.593	**104.9**
$(UO_2)_3(OH)_7^-$					-32.2		-31.0508		-30.18		-31.0508			
$(UO_2)_3(OH)_8^{2-}$									-37.65					
$(UO_2)_3(OH)_{10}^{2-}$									-62.4					
$(UO_2)_4(OH)_7^+$					-21.9		-21.9508		-21.9		-21.9508			
$UO_2CO_3^0$	9.4	**4.6**	9.4	**4.6**	9.94	**5.0**	9.6654	**-0.4**	9.68	**1.5**	9.6654	**5.0**	10.071	**3.5**
$UO_2(CO_3)_2^{2-}$	16.4	**14.6**	16.4	**14.6**	16.61	**18.5**	16.9109	**9.8**	16.95	**11.1**	16.9109	**18.5**	17.008	**14.6**
$UO_2(CO_3)_3^{4-}$	21.6	**-38.9**	21.6	**-38.9**	21.84	**-39.2**	21.5562	**-50.5**	21.61	**-49.9**	21.5562	**-39.2**	21.384	**-36.7**
$(UO_2)_3(CO_3)_6^{6-}$					54	**-62.7**	53.9127	**-92.2**	54.01	**-84.4**	53.9127	**-62.7**		
$Ca_2UO_2(CO_3)_3^0$			29.82		30.7				30.7					

Table S1. (contd.)

Model/database combination	WHAM-d[a,b]		WHAM-m[a,b]		VMIN-d, GWB-m		CHESS-ch[c,d], GWB-c[c,d]		CHESS-ct[c,d]		PHREEQC-l[c,d]		PHREEQC-m[b]	
Database name	default		modified		v3.0		chess.tdb, thermo.com.v8.r6+		ctdpv3_Dong.tdb		llnl		minteq	
Complex	log *K*, 25ºC	ΔH, kJ/mol	log *K*, 25ºC	ΔH, kJ/mol	log *K*, 25ºC	ΔH, kJ/mol	log *K*, 25ºC	ΔH, kJ/mol	log *K*, 25ºC	ΔH, kJ/mol	log *K*, 25ºC	ΔH, kJ/mol	log *K*, 25ºC	ΔH, kJ/mol
$CaUO_2(CO_3)_3^{2-}$			26.37		27.18				27.18					
$MgUO_2(CO_3)_3^{2-}$			25.3						25.8					
$(UO_2)_2CO_3(OH)_3^-$			-0.851				-0.8941		-0.85		-0.8941			
$(UO_2)_3O(OH)_2(HCO_3)^+$			0.609				0.6159		0.66		0.6159			
$(UO_2)_3(OH)_5CO_2^+$							0.7094				0.7094			
$(UO_2)_{11}(CO_3)_6(OH)_{12}^{2-}$			36.2381				36.2381				36.2381			
$UO_2NO_3^+$					0.3	**-12**	0.2805		0.3		0.2805			
$UO_2SO_4^0$	3		3		3.15	**19.5**	3.0703	**16.5**	3.15	**19.2**	3.0703	**19.8**	2.709	**21.3**
$UO_2(SO_4)_2^{2-}$	4.14		4.14		4.14	**35.1**	3.9806	**28.5**	4.14	**34.7**	3.9806	**35.6**	4.183	**25.5**
$UO_2(SO_4)_3^{4-}$	3.02		3.02						2.62					
$(UO_2)_2(OH)_2(SO_4)_2^{2-}$									-0.69					
$(UO_2)_3(OH)_4(SO_4)_4^{6-}$									-6					
$(UO_2)_4(OH)_7(SO_4)_4^{7-}$									-19.01					
$UO_2PO_4^-$	13.23		13.23		13.23		14.4016		13.21		14.4016			
$UO_2HPO_4^0$	19.615		19.615		19.615		20.7616		19.62		20.7616		20.814	**-8.8**
$UO_2H_2PO_4^+$	20.693		20.693		20.693		23.9937		22.75		23.9937		22.643	**-15.5**
$UO_2H_3PO_4^{2+}$	22.481		22.481		22.481		23.6337		22.43		23.6337			
$UO_2(HPO_4)_2^{2-}$													42.988	**-47.693**

Table S1. (contd.)

Model/database combination	WHAM-d[a,b]		WHAM-m[a,b]		VMIN-d, GWB-m		CHESS-ch[c,d], GWB-c[c,d]		CHESS-ct[c,d]		PHREEQC-l[c,d]		PHREEQC-m[b]	
Database name	default		modified		v3.0, thermo.minteq		chess.tdb, thermo.com.v8.r6+		ctdpv3_Dong.tdb		llnl		minteq	
Complex	log *K*, 25ºC	ΔH, kJ/mol	log *K*, 25ºC	ΔH, kJ/mol	log *K*, 25ºC	ΔH, kJ/mol	log *K*, 25ºC	ΔH, kJ/mol	log *K*, 25ºC	ΔH, kJ/mol	log *K*, 25ºC	ΔH, kJ/mol	log *K*, 25ºC	ΔH, kJ/mol
$UO_2(H_2PO_4)_3^-$													66.245	**-119.7**
$UO_2(H_2PO_4)(H_3PO_4)^+$							47.3973		44.99		47.3973			
$UO_2(H_2PO_4)_2^0$							46.3873		44.84		46.3873		44.7	**-69.0**
$UO_2H_3SiO_4^+$					-1.9111								-2.4	
UO_2Cl^+	0.17	**8**	0.17	**8**	0.17	**8**	0.1572	**5.9**	0.17	**8**	0.1572	**8.0**	0.22	**5.2**
$UO_2Cl_2^0$	-1.1	**15**	-1.1	**15**	-1.1	**15**	-1.1253	**13.7**	-1.1	**15**	-1.1253	**15.0**		
UO_2F^+	5.16	**1.7**	5.16	**1.7**	5.16	**1.7**	5.0502	**-0.3**	5.09	**1.9**	5.0502	**1.7**	5.105	**-1.9**
$UO_2F_2^0$	8.83	**2.1**	8.83	**2.1**	8.83	**2.1**	8.5403	**-1.7**	8.62	**1.9**	8.5403	**2.1**	8.92	**-3.8**
$UO_2F_3^-$	10.9	**2.51**	10.9	**2.51**	10.9	**2.35**	10.7806	**-0.6**	10.9	**2.5**	10.7806	**2.3**	11.364	**-3.6**
$UO_2F_4^{2-}$	11.84	**0.3**	11.84	**0.3**	11.84	**0.29**	11.5407	**-4.8**	11.7	**0**	11.5407	**0.28**	12.607	**-4.6**

Table S1. contd.

Model/database combination	WHAM-d[a,b], WHAM–m[a,b]		VMIN-d, GWB–m		CHESS-ch[c,d], GWB-c[c,d]		CHESS-ct[c,d]		PHREEQC-l[c,d]	
Database name	default, modified		v3.0, thermo.minteq		chess.tdb, thermo.com.v8.r6+		ctdpv3_Dong.tdb		llnl	
Complex	log *K*, 25ºC	ΔH, kJ/mol	log *K*, 25ºC	ΔH, kJ/mol	log *K*, 25ºC	ΔH, kJ/mol	log *K*, 25ºC	ΔH, kJ/mol	log *K*, 25ºC	ΔH, kJ/mol
$ThOH^{3+}$	-2.34	**20.74**	-3.197	**22.81**	-3.8871	**25.53**	-3.80	**24.84**		
$Th(OH)_2^{2+}$	-6.36	**39.43**	-6.894	**57.62**	-7.1068	**59.73**	-7.02	**59.03**	-7.1068	**58.668**
$Th(OH)_3^{+}$	-11.7	**59.69**			-11.8623		-11.77			
$Th(OH)_4^{0}$	-15.9	**88.06**			-16.0315	**100.77**	-15.94	**106.23**		
$Th_2(OH)_2^{6+}$			-6.094	**61.62**	-6.4618	**65.92**	-6.26	**64.54**		
$Th_4(OH)_8^{8+}$					-21.7568	**253.15**	-21.41	**250.38**		
$Th_6(OH)_{15}^{9+}$					-37.7027	**472.53**	-37.18	**468.38**		
$ThCO_3^{2+}$	11.03									
$Th(CO_3)_5^{6-}$	31		32.3				32.33			
$Th(OH)_2(CO_3)_3^{4-}$	30.8									
$Th(OH)_3CO_3^{-}$	40.1		-0.5				41.47			
$ThSO_4^{2+}$	6.17	**20.92**			5.3143	**11.67**	5.40	**10.97**		
$Th(SO_4)_2^{0}$	9.69	**40.38**			9.617	**25.11**	9.71	**30.57**		
$Th(SO_4)_3^{2-}$	10.748				10.4014		10.49			
$Th(SO_4)_4^{4-}$					8.4003		8.49			
$ThCl^{3+}$	1.18		1.38		0.9536	**-2.02**	1.04	**-2.71**		
$ThCl_2^{2+}$					0.6758		0.76			
$ThCl_3^{+}$					1.4975		1.59			
$ThCl_4^{0}$					1.0731		1.16			
ThF^{3+}	8.44		8.65	**1**	7.8725	**-6.73**	7.96	**-7.43**		
ThF_2^{2+}	15.06		15.26	**4.1**	14.0884	**-11.57**	14.18	**-12.27**		
ThF_3^{+}			20.2	**7.9**	18.7357	**-17.52**	18.82	**-18.21**		
ThF_4^{0}			23.2		22.1515	**-22.86**	22.24	**-17.42**		

Table S1. contd.

Model/database combination	WHAM-d[a,b], WHAM–m[a,b]		VMIN-d, GWB–m		CHESS-ch[c,d], GWB-c[c,d]		CHESS-ct[c,d]		PHREEQC-l[c,d]	
Database name	default, modified		v3.0, thermo.minteq		chess.tdb, thermo.com.v8.r6+		ctdpv3_Dong.tdb		llnl	
Complex	log *K*, 25ºC	ΔH, kJ/mol	log *K*, 25ºC	ΔH, kJ/mol	log *K*, 25ºC	ΔH, kJ/mol	log *K*, 25ºC	ΔH, kJ/mol	log *K*, 25ºC	ΔH, kJ/mol
$ThNO_3^{3+}$			1.75							
$Th(HPO_4)_2^0$					47.3375	**-56.36**			47.3375	**-43.0576**
$Th(HPO_4)_3^{2-}$					68.1548				68.1548	
$ThH_2PO_4^{3+}$					24.0279					
$ThH_3PO_4^{4+}$					23.4415					
$ThHPO_4^{2+}$					23.0017					
$Th(OH)_4PO_4^{3-}$							-27.22			
$Th(H_2PO_4)_2^{2+}$					57.8506				47.8506	

[a] Uranyl hydrolysis product formation data have been converted to refer to the generic reaction schema $nUO_2^{2+} + mH_2O \Leftrightarrow (UO_2)_m(OH)_n^{2n-m}$. Conversion used the log *K*, 25ºC and ΔH values in the same database.

[b] Reaction enthalpy data have been converted from kcal/mol to kJ/mol using a factor of 1 kcal = 4.184 kJ.

[c] Uranyl carbonate and uranyl hydroxy–carbonate complex formation data have been converted to refer to CO_3^{2-}, not HCO_3^{2-}, as the reacting ligand. Conversion was done using the parameters for the reaction $HCO_3^- \Leftrightarrow H^+ + CO_3^{2-}$ present in the same database.

[d] Data for formation of phosphate complexes converted to refer to PO_4^{3-}, not HPO_4^{3-}, as the reacting ligand. Conversion was done using the parameters for the reaction $HPO_4^{2-} \Leftrightarrow H^+ + PO_4^{3-}$ present in the same database.

[e] Value in database (0.9 kJ/mol) deemed incorrect so not used.

2. Modelling the binding of uranyl and thorium to hydrous ferric oxide in WHAM7

The model used for ion binding to HFO is that of Lofts and Tipping (1998), and unless otherwise stated, all model parameters used in this study are taken from that study. Proton binding to hydrous ferric oxide is considered using a two–*K* model:

$$\equiv \mathrm{FeOH_2^+} \quad \Leftrightarrow \quad \equiv \mathrm{FeOH} + \mathrm{H^+};\ \frac{[\equiv \mathrm{FeOH}]\cdot a_{\mathrm{H}}}{[\equiv \mathrm{FeOH_2^+}]} = \mathrm{K_{H_1}} \exp\left(2wZ\right)$$

$$\equiv \mathrm{FeOH} \quad \Leftrightarrow \quad \equiv \mathrm{FeO^-} + \mathrm{H^+};\ \frac{[\equiv \mathrm{FeO^-}]\cdot a_{\mathrm{H}}}{[\equiv \mathrm{FeOH}]} = \mathrm{K_{H_2}} \exp\left(2wZ\right)$$

Binding of other cations is simulated by monodentate metal–proton exchange:

$$\equiv \mathrm{FeOH} + \mathrm{M^{z+}} \quad \Leftrightarrow \quad \equiv \mathrm{FeOM^{(z-1)+}} + \mathrm{H^+};\ \frac{[\equiv \mathrm{FeOM^{(z-1)+}}]\cdot a_{\mathrm{H}}}{[\equiv \mathrm{FeOH}]\cdot a_{\mathrm{M}}} = \mathrm{K_{MH}} \exp\left(-2w(z-1)Z\right)$$

and binding of anions by monodentate ligand exchange:

$$\equiv \mathrm{FeOH} + n\mathrm{H^+} + \mathrm{A^{y-}} \quad \Leftrightarrow \quad \equiv \mathrm{FeH_{\mathit{n}\text{-}1}A^{(\mathit{y}-\mathit{n})-}} + \mathrm{H_2O};\ \frac{[\equiv \mathrm{FeH_{\mathit{n}\text{-}1}A^{(\mathit{n}\text{-}\mathit{y})+}}]}{[\equiv \mathrm{FeOH}]\cdot a_{\mathrm{A}}\cdot a_{\mathrm{H}}^{n}} = \mathrm{K_{AH}} \exp\left(-2w(n-y)Z\right)$$

or

$$\equiv \mathrm{FeOH} + \mathrm{A^{y-}} \quad \Leftrightarrow \quad \equiv \mathrm{FeOHA^{y-}};\ \frac{[\equiv \mathrm{FeOHA^{y-}}]}{[\equiv \mathrm{FeOH}]\cdot a_{\mathrm{A}}} = \mathrm{K_{AH}} \exp\left(2wyZ\right)$$

The K terms are intrinsic equilibrium constants, which describe the binding strength to an uncharged surface. The exponential terms quantify the electrostatic component of the binding strength, with the term Z being the surface charge of the oxide (eq g^{-1}) and *w* being an electrostatic term where

$$w = \frac{\mathrm{P_A}\cdot \log_{10} I}{\mathrm{SSA}}$$

the term *I* being the bulk solution ionic strength (mol dm^{-3}), SSA is the oxide surface area in $m^2\ g^{-1}$ and P_A is a fitted electrostatic parameter.

The equilibrium expression for cation or anion binding can be generalised to:

$$\equiv \mathrm{S} + \mathrm{X^{\mathit{x}}} + m\mathrm{H^+} \quad \Leftrightarrow \quad \equiv \mathrm{S'X^{\mathit{x}+\mathit{m}}};\ \frac{[\equiv \mathrm{S'X^{\mathit{x}+\mathit{m}}}]}{[\equiv \mathrm{S}]\cdot a_{\mathrm{X}}\cdot a_{\mathrm{H}}^{m}} = \mathrm{K_{XH}} \exp\left(-2w(x+m)Z\right)$$

where *m* is the proton stoichiometry of the reaction, which can take both positive and negative values (*m* = -1 for cations, $m \geq 0$ for anions), X is the binding ion, ≡S represents the neutral ≡FeOH surface species and ≡S' represents either ≡FeO, ≡Fe or ≡FeOH, depending upon the stoichoimetry of proton interaction.

Heterogeneity of binding site strengths for cations is represented by having three surface binding site types, denoted 0,1 and 2, with binding constants given by

$$\mathrm{pK}_{\mathrm{MH},y} = \mathrm{pK}_{\mathrm{MH}} + y \cdot \Delta\mathrm{pK}_{\mathrm{MH}}$$

where $y = 0$ for 90.1% of the binding sites, $y = 1$ for 9.0% of the sites and $y = 2$ for 0.9% of the sites. The term $\Delta\mathrm{pK}_{\mathrm{MH}}$ is a heterogeneity term. In the work of Lofts and Tipping (1998), where only cation binding was considered, a values of -2 for $\Delta\mathrm{pK}_{\mathrm{MH}}$ was adopted for all cation binding to HFO. This provides a range of binding site affinities, with the less–abundant sites having higher affinities. Anion binding strength is assumed the same for all the site types, i.e. there is no heterogeneity of binding strength.

The surface reactions give rise to a charge on the oxide surface. Counterions may bind electrostatically by diffuse accumulation adjacent to the surface, in response to this charge. Counterion concentrations are calculated using the expression

$$\frac{c_D(\mathrm{i})}{c_S(\mathrm{i})} = \mathrm{K}_{\mathrm{sel}}(\mathrm{i}) R^{|z(\mathrm{i})|}$$

where $c_s(\mathrm{i})$ and $c_D(\mathrm{i})$ are the concentrations of counterion *i* in the diffuse layer and bulk solution, respectively, $\mathrm{K}_{\mathrm{sel}}(\mathrm{i})$ is a selectivity coefficient for *i* and *z*(i) is the charge on *i*. The parameter *R* is a ratio term which is optimised such that the charge due to counterion accumulation balances the surface charge. In this work, as in Lofts and Tipping (1998), all $\mathrm{K}_{\mathrm{sel}}(\mathrm{i})$ values were set to unity, i.e. counterion accumulation was a function of ionic charge only.

Optimisation of binding constants for CO_3^{2-} and uranyl species

Initial fitting suggested an important role for carbonate as a competing ion at high pH. Possible effects of carbonate are:

1. Competition as a solution ion for uranyl with HFO;
2. Ternary binding of uranyl–carbonate complexes;
3. Competitive binding of carbonate and uranyl to the HFO surface.

The first possibility is automatically accounted for by including carbonate in the speciation calculations, while the second may be accounted for by allowing uranyl–carbonate complexes to

adsorb to HFO. Accounting for the third possibility requires parameterisation of the model for carbonate binding to HFO in the absence of uranyl; thus we first parameterised the model for carbonate binding and fixed the derived parameters in the uranyl fitting efforts.

General considerations

All model parameters apart from the CO_3^{2-} and uranyl binding constants were taken from Lofts and Tipping (1998) (Table S2).

Table S2. Basic physicochemical parameters for the HFO surface complexation model. All values are from Lofts and Tipping (1998).

Parameter	Units	Value
Bulk density	kg m^{-3}	3.57×10^{6}
pK_{H1}	–	6.26
pK_{H2}	–	9.66
Site density	mol m^{-2}	8.33×10^{-6}
SSA	m^2 g^{-1}	600
P_A	–	-1.46×10^{6}
ΔpK_{MH}	–	-2

Optimisation of CO_3^{2-} binding

Parameters for carbonate binding to HFO were obtained by fitting to the data of Zachara et al. (1987), which comprised two pH adsorption edges with HFO concentrations of 0.78 and 7.8 g dm^{-3} respectively and total carbonate concentration fixed to 4.6×10^{-6} mol dm^{-3}. The model fits are shown in Figure 1. A single surface reaction was used:

$$\equiv \mathrm{FeOH} + \mathrm{H^+} + \mathrm{CO_3^{2-}} \quad \Leftrightarrow \quad \equiv \mathrm{FeOCO_2^-} + \mathrm{H_2O}$$

Binding site heterogeneity was not invoked for anion binding, following Dzombak and Morel (1990), so ΔpK_{XH} was set to zero. An optimised pK_{AH} of -11.85 was computed. Addition of further binding reactions did not improve the fit. The model fit is shown in Figure S1.

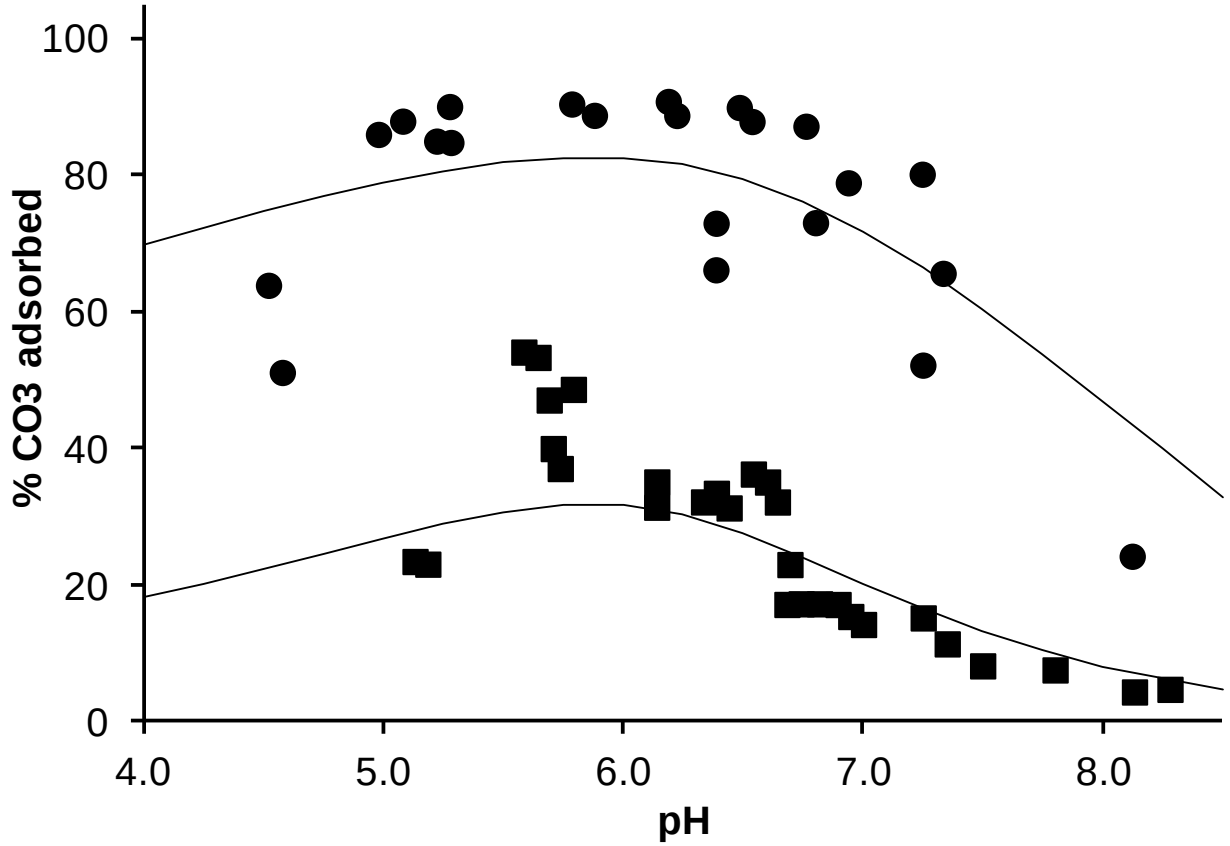

Figure S1. Model fits to the carbonate–HFO binding data of Zachara et al. (1987). Ionic strength = 0.1 mol dm^{-3}, total CO_3 = 4.6 × 10^{-6} mol dm^{-3}. HFO = 0.78 g dm^{-3} (circles), 7.8 g dm^{-3} (squares).

Optimisation of uranyl binding

Existing literature datasets on uranyl binding to HFO were collated from the literature (Table S3). A single parameter fit was made to all datasets. Where only % UO_2 adsorption data were available, rather than direct measurements of dissolved uranyl, points representing less than 20% or greater than 80% adsorption were removed, to avoid errors in deriving dissolved urnayl concentrations. The total number of data points found was 289, of which 165 points were suitable for fitting.

Fitting was done by minimising the sum of squares error in the log dissolved uranyl concentrations. Following Lofts and Tipping (1998), we initially postulated that the binding species comprised the uranyl free ion (UO_2^{2+}) and its first hydrolysis product (UO_2^{2+}). Initial fitting suggested a need to include additional carbonate binding species, e.g. $UO_2CO_3^0$, as has been done by other authors (e.g. Waite et al., 1994, Mahoney et al., 2009). This produced an optimised set of binding reactions and constants:

$$\equiv \mathrm{FeOH} + \mathrm{UO_2^{2+}} \quad \Leftrightarrow \quad \equiv \mathrm{FeOUO_2^{+}} + \mathrm{H^{+}};\ \mathrm{pK_{MH}} = 3.60$$

$$\equiv \mathrm{FeOH} + \mathrm{UO_2OH^{+}} \quad \Leftrightarrow \quad \equiv \mathrm{FeOUO_2OH^{0}} + \mathrm{H^{+}};\ \mathrm{pK_{MH}} = 1.89$$

$$\equiv FeOH + UO_2CO_3^0 \quad \Leftrightarrow \quad \equiv FeOUO_2CO_3^- + H^+ ;\ pK_{MH} = 6.97$$

$$\equiv FeOH + UO_2(CO_3)_2^{2-} \quad \Leftrightarrow \quad \equiv FeOUO_2(CO_3)_2^{3-} + H^+ ;\ pK_{MH} = 4.23$$

The RMSE in log dissolved uranyl was 0.34.

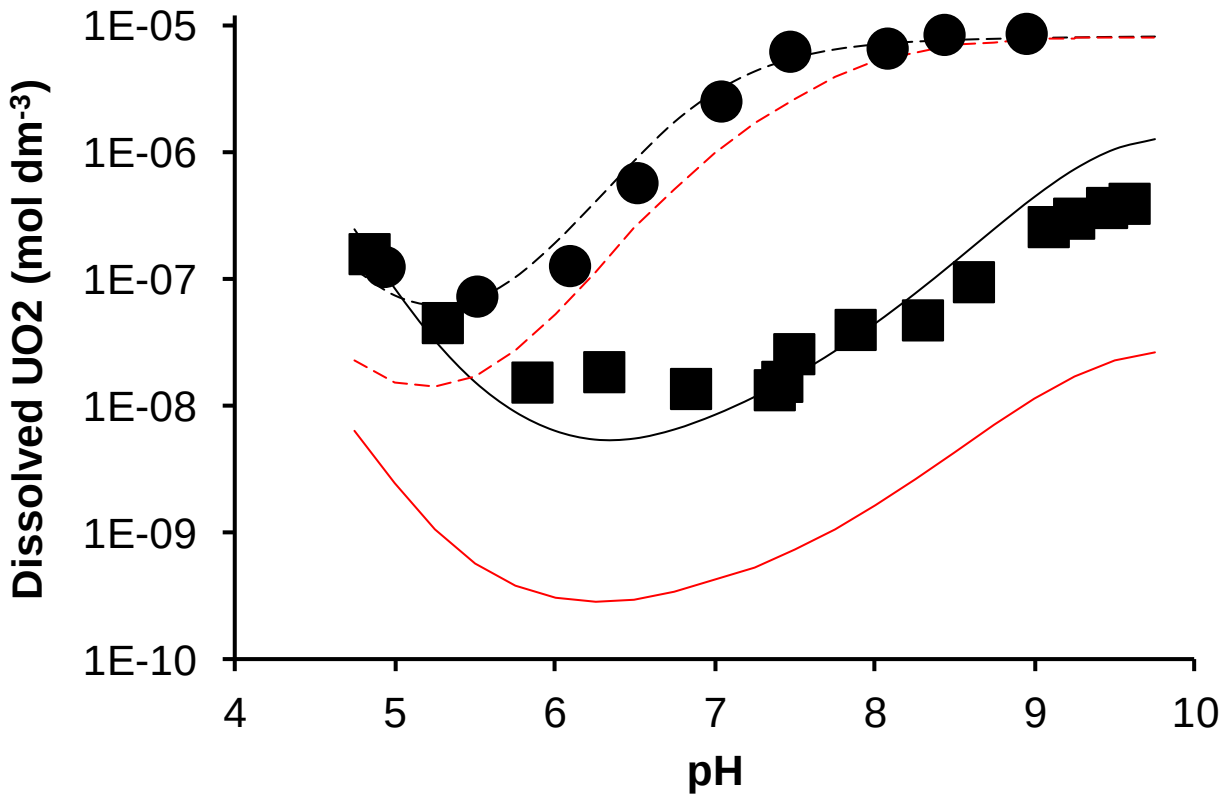

Figure S2 and Figure S3 show example model predictions, including data points not used for fitting, and for comparison predictions of uranyl binding to HFO predicted using the binding constants estimated by the linear free energy relationship of Lofts and Tipping (1998), as used in the WHAM–d predictions.

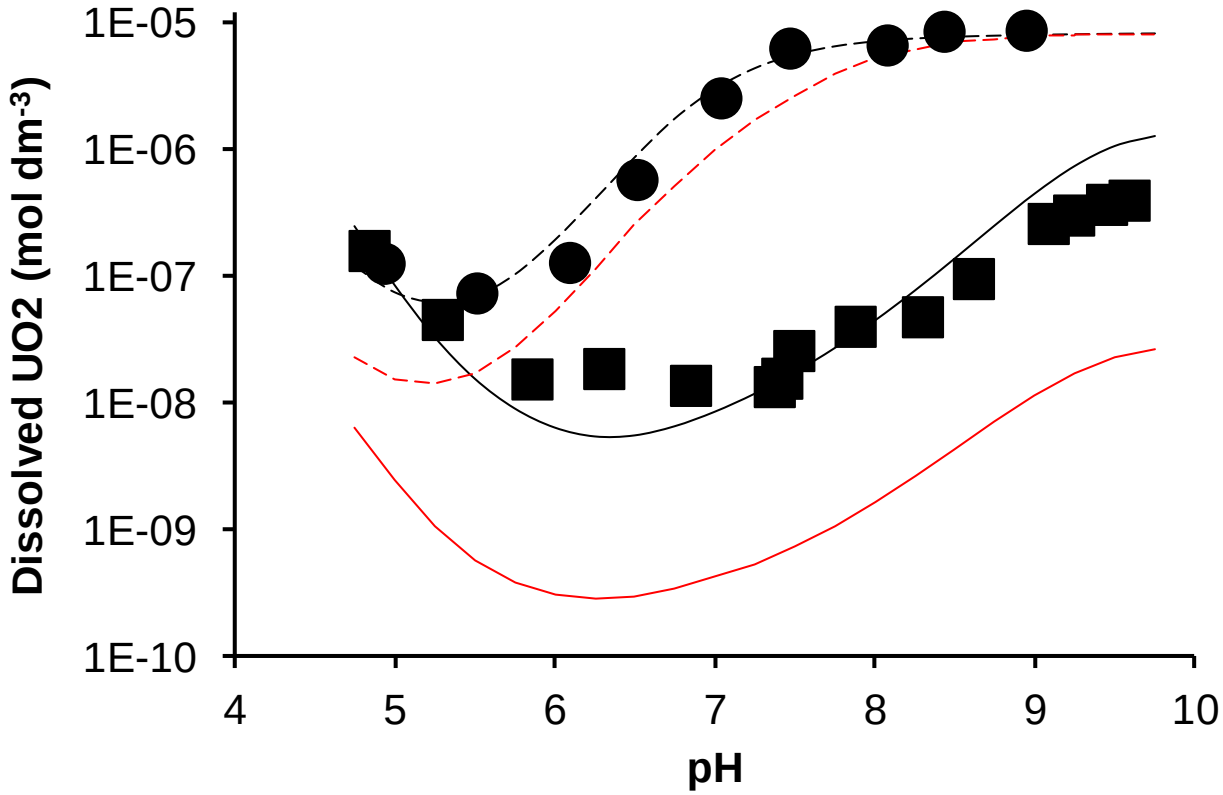

Figure S2. Model fit to datasets $FeUO_2$–3a (squares, solid lines) and $FeUO_2$–3b (circles, dashed lines). Points are the observed variation in dissolved uranyl with pH (see Table S3 for experimental conditions). The black line is the universal model fit. The red lines are predictions obtained using binding constants estimated from the linear free energy relationship of Lofts and Tipping (1998).

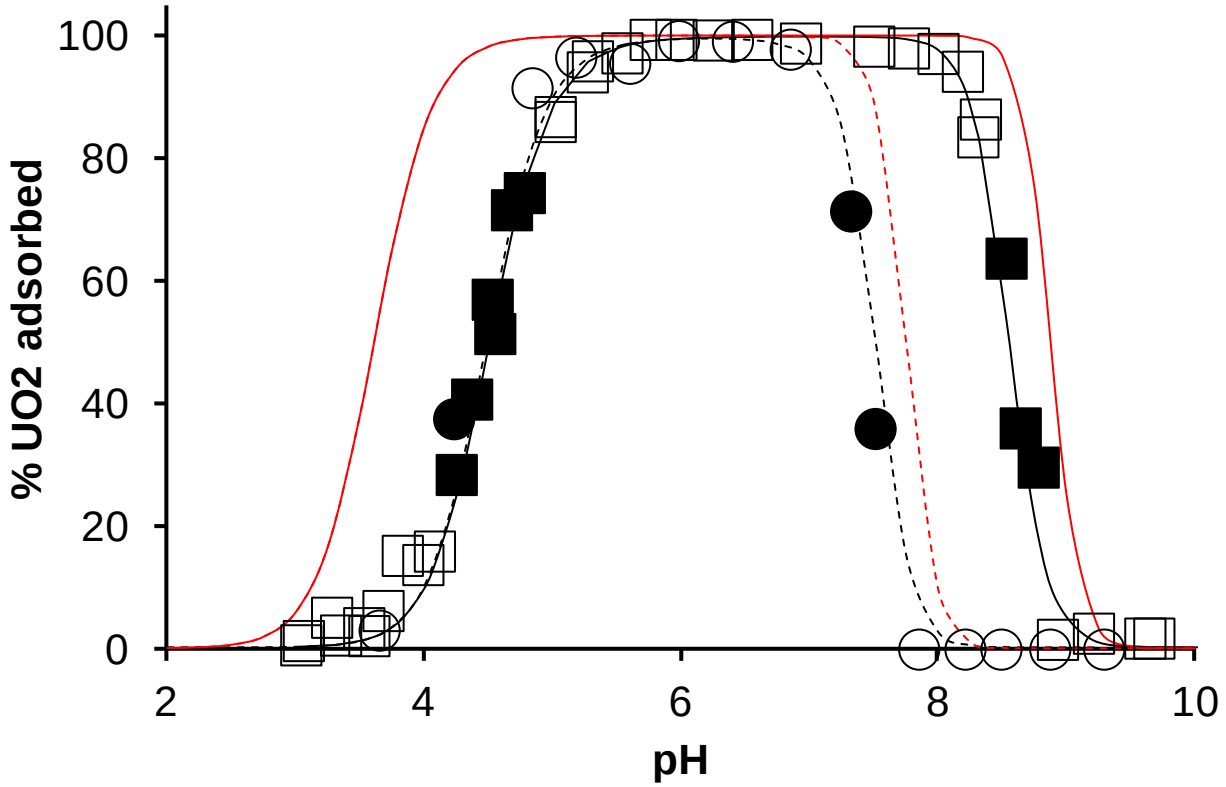

Figure S3. Model fit to datasets $FeUO_2$–2g (squares, solid lines) and $FeUO_2$–2j (circles, dashed lines). See Table S1 for experimental conditions. Closed symbols are those data points used in the universal fitting, open symbols are data points not used in fitting. Black lines are model predictions using the universally–fitted binding constants, red lines are predictions using the binding constants derived from the linear free energy relationship of Lofts and Tipping (1998).

Optimisation of thorium binding

Thorium binding was optimised using the data of Rojo et al. (2009), who presented three pH adsorption envelopes for Th on HFO in the pH range 1.5–4.5. Three concentrations of thorium – 0.95µM, 1.1µM and 1.7µM – were used, and an HFO concentrations HFO of 10 g dm^{-3}. The background electrolyte was $NaClO_4$ and the ionic strength was 0.01M when the thorium concentration was 0.95µM or 1.7 µM, and 0.1M when the thorium concentration was 1.1µM. The experiments were done open to the atmosphere, A total of 14 points were suitable for fitting.

Prediction of Th^{4+}/$ThOH^{3+}$ binding was underestimated using the default pK_{MH} value of -2.3 computed by Lofts and Tipping (1998). Optimisation, keeping the pK_{MH} value for both Th^{4+} and $ThOH^{3+}$ equal, produced a value of -5.12. The data are presented in Figure S5, along with default and optimised model lines.

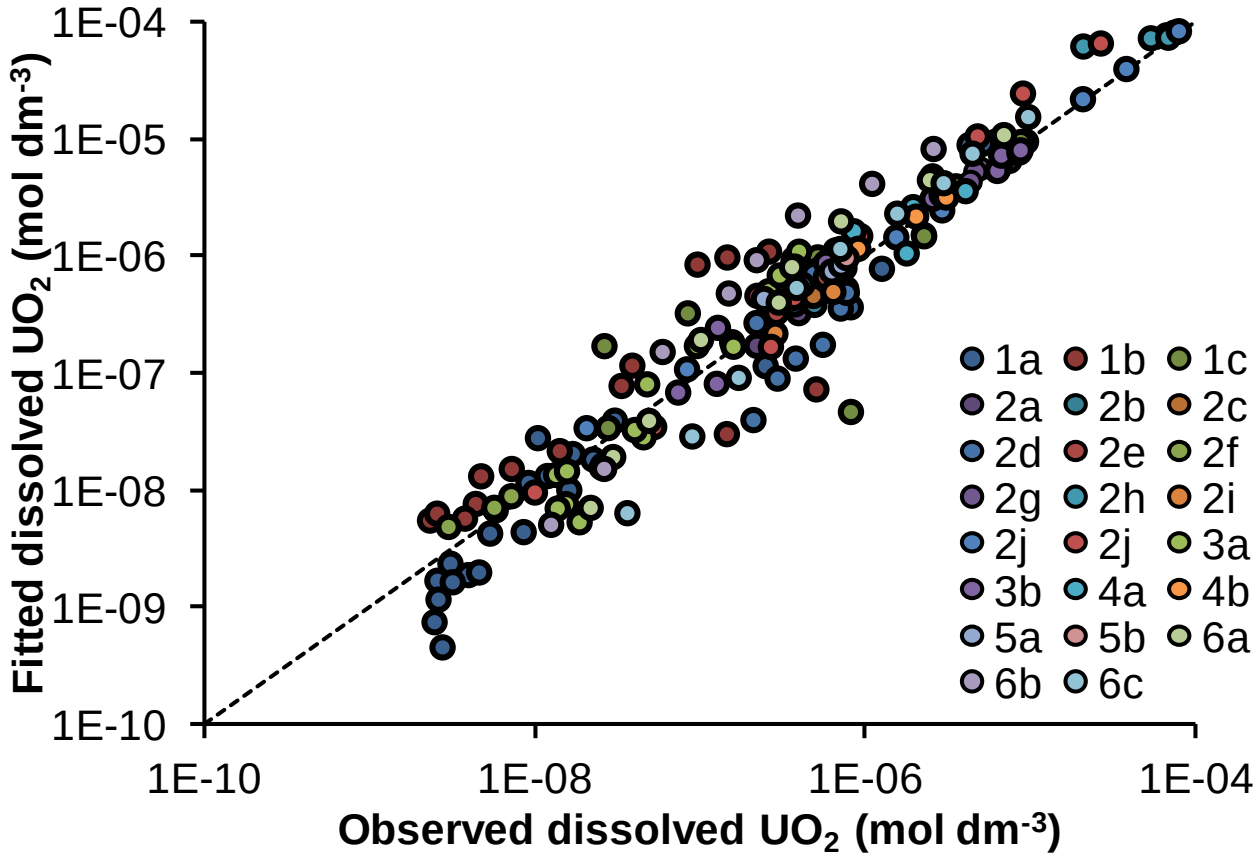

Figure S4. Modelled dissolved UO_2 calculated by fitting, plotted against observed dissolved UO_2 for all data points (n = 169) used in fitting HFO binding constants.

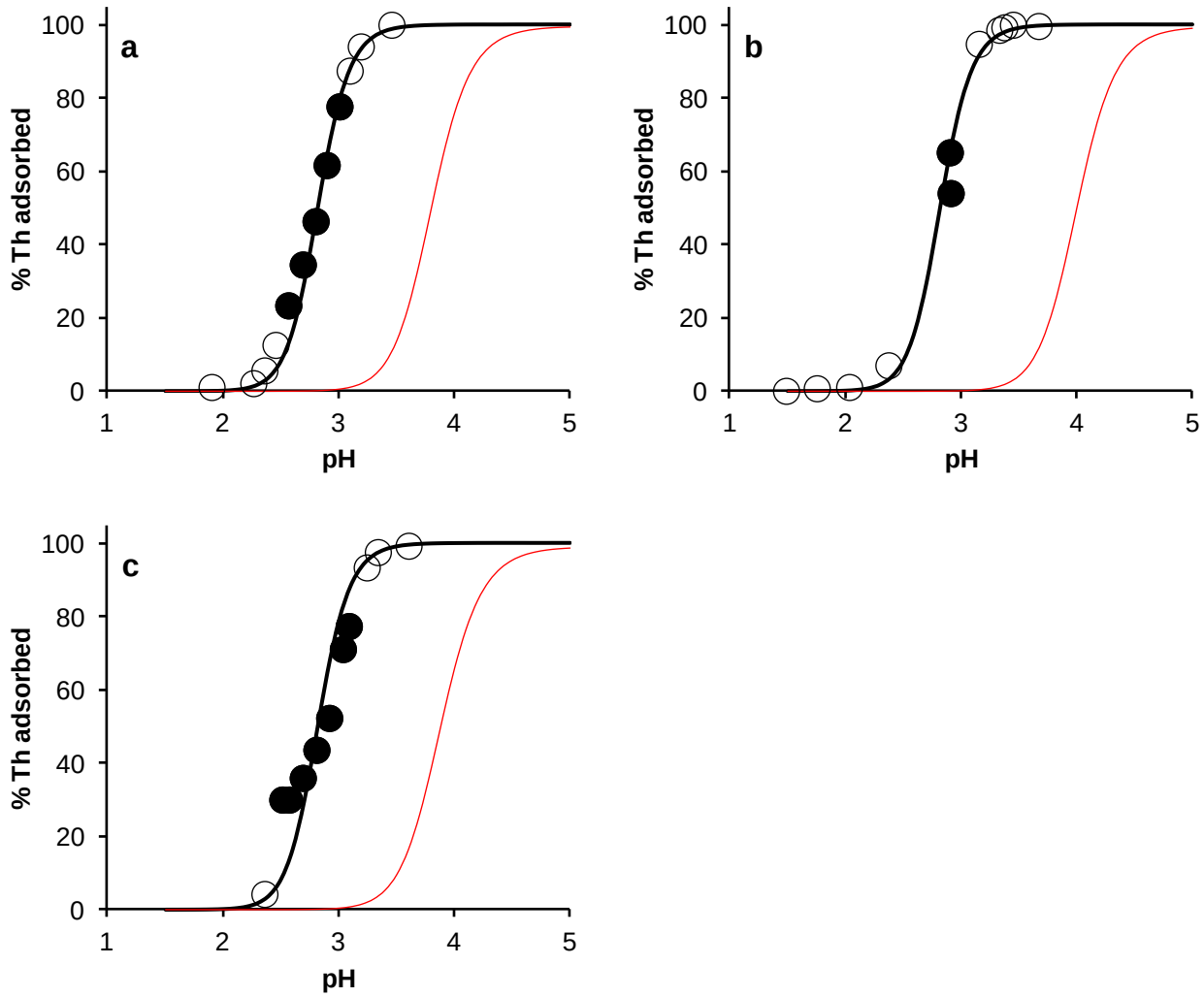

Figure S5. Model descriptions of the pH adsorption envelopes of Rojo et al. (2009), using default constants (red lines) and fitted constants (black lines). Solid points are those used in fitting, open points were not used in fitting. a: 0.95 µM Th, I = 0.01M $NaClO_4$; b: 1.1 µM Th, I = 0.1M $NaClO_4$; c: 1.7 µM Th, I = 0.01M $NaClO_4$. The concentration of HFO was 10 g dm^{-3} throughout.

Table S3. Datasets used for fitting of UO_2 binding to HFO.

Reference	Experiment type	*n* total	*n* used for fitting	Total UO_2 mol dm^{-3}	Total HFO g dm^{-3}	Ionic strength mol dm^{-3}	pH	Carbonate system	Reference
$FeUO_2$–1a	Adsorption edge	28	28	10^{-5}	1	0.1	3.3–9.6	$T_{CO3} = 0$	Hsi & Langmuir 1985
$FeUO_2$–1b	Adsorption edge	15	15	10^{-5}	1	0.1	5.0–9.8	$T_{CO3} = 10^{-3}$ mol dm^{-3}	Hsi & Langmuir 1985
$FeUO_2$–1c	Adsorption edge	12	12	10^{-5}	1	0.1	3.2–9.7	$T_{CO3} = 10^{-2}$ mol dm^{-3}	Hsi & Langmuir 1985
$FeUO_2$–2a	Adsorption edge	7	4	10^{-6}	0.09	0.004	3.6–5.2	$pCO_2 = 10^{-3.5}$ atm	Waite et al. 1994; Payne, 1999
$FeUO_2$–2b	Adsorption edge	18	6	10^{-6}	0.09	0.02	3.5–9.2	$pCO_2 = 10^{-3.5}$ atm	Waite et al. 1994; Payne, 1999
$FeUO_2$–2c	Adsorption edge	40	9	10^{-6}	0.09	0.1	3.5–9.7	$pCO_2 = 10^{-3.5}$ atm	Waite et al. 1994; Payne, 1999
$FeUO_2$–2d	Adsorption edge	18	9	10^{-6}	0.09	0.5	3.6–9.1	$pCO_2 = 10^{-3.5}$ atm	Waite et al. 1994; Payne, 1999
$FeUO_2$–2e	Adsorption edge	20	4	10^{-6}	1.8	0.1	3.6–9.3	$pCO_2 = 10^{-3.5}$ atm	Waite et al. 1994; Payne, 1999
$FeUO_2$–2f	Adsorption edge	5	3	10^{-8}	0.09	0.1	4.0–5.1	$pCO_2 = 10^{-3.5}$ atm	Waite et al. 1994; Payne, 1999
$FeUO_2$–2g	Adsorption edge	18	6	10^{-5}	0.09	0.1	3.9–6.7	$pCO_2 = 10^{-3.5}$ atm	Waite et al. 1994; Payne, 1999
$FeUO_2$–2h	Adsorption edge	17	5	10^{-4}	0.09	0.1	3.9–8.7	$pCO_2 = 10^{-3.5}$ atm	Waite et al. 1994; Payne, 1999
$FeUO_2$–2i	Adsorption edge	15	3	10^{-6}	0.09	0.1	3.6–9.3	$pCO_2 = 10^{-2}$ atm	Waite et al. 1994; Payne, 1999
$FeUO_2$–2j	pH isotherm	11	11	$10^{-7.02}$–$10^{-3.53}$	0.09	0.02	4.5	$pCO_2 = 10^{-3.5}$ atm	Payne, 1999
$FeUO_2$–2k	pH isotherm	13	13	$10^{-6.52}$–$10^{-3.02}$	0.09	0.02	5.25	$pCO_2 = 10^{-3.5}$ atm	Payne, 1999
$FeUO_2$–3a	Adsorption edge	15	15	10^{-5}	1	0.1	4.8–9.6	$T_{CO3} = 10^{-3}$ mol dm^{-3}	Morrison et al. 1995
$FeUO_2$–3b	Adsorption edge	9	9	$10^{-5.08}$	0.52	0.1	4.9–9.0	$T_{CO3} = 0.0195$ mol dm^{-3}	Morrison et al. 1995
$FeUO_2$–4a	Adsorption edge	16	5	$10^{-5.38}$	0.128	0.1	3.4–9.6	$T_{CO3} = 10^{-2}$ mol dm^{-3}	Wazne et al. 2003
$FeUO_2$–4b	Adsorption edge	17	3	$10^{-5.38}$	0.128	0.1	3.0–9.9	$T_{CO3} = 10^{-5}$ mol dm^{-3}	Wazne et al. 2003
$FeUO_2$–5a	Adsorption edge	9	4	10^{-6}	0.009	0.0109	6.9–8.5	$pCO_2 = 10^{-3.37}$ atm	Fox et al. 2006
$FeUO_2$–5b	Adsorption edge	7	2	10^{-6}	0.9	0.005	6.5–8.2	$pCO_2 = 10^{-1.7}$ atm	Fox et al. 2006
$FeUO_2$–6a	pH isotherm	9	9	$10^{-6.80}$–$10^{-4.84}$	0.009	0.001	5.9	$pCO_2 = 10^{-3.5}$ atm	Jang et al. 2007
$FeUO_2$–6b	pH isotherm	8	8	$10^{-6.55}$–$10^{-4.95}$	0.009	0.001	6.8	$pCO_2 = 10^{-3.5}$ atm	Jang et al. 2007
$FeUO_2$–6c	pH isotherm	9	9	$10^{-6.75}$–$10^{-4.76}$	0.009	0.001	7.8	$pCO_2 = 10^{-3.5}$ atm	Jang et al. 2007

References

Dzombak, D.A., Morel, F.M.M., 1990. Surface Complexation Modeling: Hydrous Ferric Oxide. John Wiley & Sons, New York.

Fox, P.M., Davis, J.A., Zachara, J.M. 2006. The effect of calcium on aqueous uranium(VI) speciation and adsorption to ferrihydrite and quartz. Geochimica et Cosmochimica Acta 70:1379-1387.

Guillaumont, R., Fanghänel, T., Fuger, J., Grenthe, I., Neck V., Palmer, D.A., Rand, M.H. 2003. Update on the Chemical Thermodynamics of Uranium, Neptunium, Plutonium, Americium and Technetium. Elsevier BV, Amsterdam.

Hsi, C.–K.D., Langmuir, D.. 1985. Adsorption of uranyl onto ferric oxyhydroxide: application of the surface complexation site–binding model. Geochimica et Cosmochimica Acta 49:1931–1941.

Jang, J.H., Dempsey, B.A., Burgos, W.D. 2007. A Model-Based Evaluation of Sorptive Reactivities of Hydrous Ferric Oxide and Hematite for U(VI). Environmental Science & Technology 41:4305–4310.

Lofts S., Tipping E. 1998. An assemblage model for cation binding to particulate matter. Geochimica et Cosmochimica Acta 62:2609–2625.

Morrison, S.J., Spangler, R.R., Tripathi, V.S. 1995. Adsorption of uranium(VI) on amorphous ferric oxyhydroxide at high concentrations of dissolved carbon(IV) and sulfur(VI). Journal of Contaminant Hydrology 17:333-346.

Rojo, I., Seco, F., Rovira, M., Giménez, J., Cervantes, G., Martí, V., de Pablo, J. 2009. Thorium sorption onto magnetite and ferrihydrite in acidic conditions. Journal of Nuclear Materials 385: 474–478.

Waite, T.D., Davis, J.A., Payne, T.E., Waychunas, G.A., Xu, N. 1994. Uranium(VI) adsorption to ferrihydrite: Application of a surface complexation model. Geochimica et Cosmochimica Acta 58:5465–5478.

Wazne, M., Korfiatis, G.P., Meng, X. 2003. Carbonate Effects on Hexavalent Uranium Adsorption by Iron Oxyhydroxide. Environmental Science & Technology 37:3619-3624.

Zachara, J.M., Girvin, D.C., Schmidt, R.L., Resch, C.T. 1987. Chromate adsorption on amorphous iron oxyhydroxide in the presence of major groundwater ions. Environmental Science & Technology 21:589-594.